Chapter 3

PERIODIC MONITORING OF RIVER THERMAL PATTERN USING SATELLITE IMAGES

3.1 Introduction

The water temperature of an aquatic bodies plays an important role in regulating the rate of chemical reactions, Dissolved Oxygen (DO) concentrations, and the nutrient cycle of aquatic organisms; thus impacting the freshwater ecology (Caissie, 2006; Ling et al., 2017; Wawrzyniak et al., 2011). The river continuum concept emphasizes that the variation in water temperature is strongly linked with the longitudinal distribution of species in the fluvial system (Vannote et al., 1980; Wawrzyniak et al.,2011). If the stream temperature rises above the specified threshold limit, biological processes such as reproduction, growth, and even the rate of survival witnesses a declining trend (Eaton et al., 1995; Xin and Kinouchi, 2013). Thus, the river water temperature has an effectual impact on the water quality, particularly in those areas where endangered fish species are sensitive to water temperature flux (Handcock et al., 2006). DO has an indispensable role in the metabolic processes of aquatic organisms as well as in creature behavior and fish network structure (Magoulick and Kobza, 2003; Null et al., 2017). DO immersion fixation has an inverse association with the water temperature, such that DO has an upsurge during nighttime. However, in several rivers, the relationship does not hold true owing to photosynthesis and respiration (Loperfido et al., 2009; Null et al., 2017; Viswanathan et al., 2015). The diurnal temperature cycle is also responsible for pH fluctuation in river water. The solubility of calcite and dissolved CO_2 increments with the decline in temperature, creating a higher pH at a lower temperature (Bäckström et al.,2002; Viswanathan et al., 2015). The optimum pH range for freshwater aquatic life is 6.5-9.0, outside which the organisms may experience stress or even die (Wurts and Durborow, 1992).

The temperature of aquatic bodies is governed by several factors, i.e., such as meteorological conditions, river bed conditions, river morphology, and flow discharge. Variations of water temperature in the river can occur naturally. However, anthropogenic activities, such as point source and non-point source pollutant discharge from industrial, commercial, and housing sectors, also raise water temperatures (Caissie, 2006; Ling et al., 2017; Van Vliet et al., 2011). It can ultimately affect aquatic organisms and the resources occurring therein (Brown and Krygier, 1970). Deforestation has been distinguished as a critical parameter in influencing the river thermal system (Beschta, 1997). Global warming is also another factor in the rise in water temperature. It could be cited that the air temperature has shown an upward trend from the late 19th century and shows warming of 0.85°C over the time period 1880-2012 (Wawrzyniak et al., 2016). Moreover, due to the effect of global warming, river flow modifies, and this also affects the temperature profile of the river (Arnell 1999; Milly et al., 2005). Other meteorological conditions like wind speed, solar radiation, and humidity are additional factors because they also determine the heat exchange and fluxes at the river's surface (Caissie 2006; Mohseni& Stefan, 1999). Therefore, it is important to study and explain the air-water temperature relationship (Zhu et al., 2018). Several researchers have pointed out that river temperatures have risen above the ambient limit in various regions of the world during the 20th century (Kaushal et al., 2010; Wawrzyniak et al., 2016).

Several models predict if there is an increase in air temperature, then there will also be an increase in river water temperature (Webb 1996; Poirel et al., 2009). In the regression analysis of river temperature, air temperature is often used as the only independent variable since it can be used as a substitute for the net exchange in heat fluxes that affect the water surface. Air temperature estimates the equilibrium temperature of a watercourse.

Early investigations of river water temperatures primarily concentrated on habitat use by aquatic plants and animals. Conventional methods to measure the river water temperatures are expensive, time-consuming, and provide only point measurement information. It is also challenging to study the surface water temperature variation using these methods due to its spatial and temporal heterogeneity. Remote sensing can be an advantageous alternative in this regard. Remote sensing has been proved a revolutionary tool that could be used to attain information about an object by observing it from a distance and without coming into actual contact with it. Satellite images have a large spatial extent, and their periodic movement over the same area can be useful in temporal studies, especially for infeasible regions. Since satellites sensors can capture radiation over a broad range of the electromagnetic spectrum, other than the visible region, they can provide additional information, which otherwise is difficult to measure (Dash et al., 2002; Lamaro et al., 2013; Novo et al., 2006). Satellite mounted sensors sense the various objects in the form of a digital number (DN) of the energy reflected. The data obtained in the form of DN can be converted to an image by electro-optical conversion. Thus, we get an image of each scene covering the earth’s surface. Different satellite systems may have different types of sensors, depending upon the design and specific needs (Barrett et al., 1990). Compared with in-situ estimations, the thermal infrared remote detecting strategy gave an alluring option for estimating water temperatures and observing spatial patterns of thermal maps at different spatial scales (Ling et al., 2017). The blend of proper spatial resolution, continuous periodic coverage (16-day repeativity), and free accessibility to satellite data makes LANDSAT framework a suitable option for surface water body studies. The LANDSAT satellite arrangement permits the assemblage of a large number of images to address seasonal and inter-annual variability (Lamaro et al., 2013; Wawrzyniak et al., 2011).

Fluvial research dependent on the LANDSAT program is broad; however, water temperature analysis got little attention (Baban, 1993; Kay et al., 2005). Nowadays, several researchers are doing temperature analysis of rivers with remote sensing (Wawrzyniak et al., 2016; Lamaro et al., 2013). In this study, the thermal outline of the Ganga river has been analyzed between Mirzapur and Ghazipur stretch.

The objectives of this chapter are (i) to delineate the longitudinal and temporal variation of surface water temperature using TIR images of LANDSAT-7 and LANDSAT-8 satellites; (ii) to study the relationship between air temperature and surface water temperature; (iii) to compare between LANDSAT-7 and LANDSAT-8 estimated thermal temperature results.

3.2 Study area description

The study reach is located in the middle section of the river Ganga (Figure 3.1). It is 237 Kilometers long between Ghazipur and Mirzapur in the northern part of India in south-eastern Uttar Pradesh between the coordinates 82.32°E, 25.21°N to 83.62°E, 25.59°N. Varuna (joining at 120 kilometers from Mirzapur side) and Gomti (joining at 157.8 kilometers from Mirzapur side) are the major tributaries of river Ganga in this reach. Geomorphologically, the study reach has an average elevation of 76.19 m above mean sea level. The whole area has largely a very even topography, with low relief (Kumar et al., 2013; Rai et al., 2010; Singh, 1996). The river

Ganga in this stretch is low-lying with gentle slopes due to the neotectonic movements. The channel is a sand-bed river with large sand bars and is highly sinuous, generating a wandering pattern (Swamee et al., 2003).

Figure 3.1 Location of the studied reach between Mirzapur and Ghazipur in the middle valley of the Ganga River.

3.2.1 Climate

The climate of the study region is mainly tropical with a marked monsoonal impact. In this part, the summer season usually has a longer duration as compared to the winter season (Das et al., 2020). The region experiences mostly hot and dry summer (April-June) followed by warm and wet monsoon (July-September). Normally, this region experiences a southwest monsoon. During the rainy season, which starts from July to the end of September, about 80–90% of the total annual rainfall is received with intermittent dry periods. The southwest monsoon breaks around the first week of June at the mouth of the Ganga and advances upstream. By the end of July, the monsoon reaches the western end of the Ganga basin. In the greater part of the basin, the rainy season spreads over three months- July, August, and September; and usually, 70 to 80% of the total annual rainfall occurs during this period. The month of March and October is known as the spring and autumn season, respectively. The region receives 40, 36, and 768 mm rainfall on average during the winter, summer, and rainy seasons. The average temperature for these seasons ranges from 7.4–31.4, 18.7–43 to 21–36.9°C, respectively. In summers, the temperature at times exceeds 46°C. The high summer heat causes the air to expand and move upwards, carrying a lot of suspended pollutants into the upper atmosphere. Under a high-temperature regime, much of the pollutants suspended in the air are held a lot for a considerable period of time in the atmosphere. Some of the pollutants are brought down by raindrops and eventually are added to the surface runoff system. More than 90 % of the average annual rainfall (1050 mm) occurs in the rainy season. Wind direction primarily shifts westerly to southwesterly in October to April and easterly to northwesterly in the left-over months (Kumar et al., 2013; Pandey and Singh, 2017).

3.2.2 Land use/Land cover (LU/LC) pattern

“This region's significant LU/LC categories have been water bodies, vegetation, built-up, and bare lands. It has been noticed that the urban land cover has been increased by 62.07 km^2 from 1989 to 1997, 111.74 km^2 from 1997 to 2008, and 85.30 km^2 from 2008 to 2018. Obviously, 259.11 km^2 area of natural land cover was converted into urban built-ups from 1989 to 2018. Vegetation of the area was observed as the dominant area among the natural land cover across the city. The contribution of bare soil percentage was high in 1989 (i.e. 32.52%), and a substantial decrease was found in 1997 (i.e. 11.88%). The development of irrigation systems with advanced technology has proved a boon for various areas of bare land by converting it into vegetated agricultural areas. The Indo-Dutch Tubewell Project constructed various tubewells during the period 1988 to 1993 thus increasing the area for irrigation for enhanced agricultural productivity. The Free Boring Scheme in Uttar Pradesh started in 1984 and reached 2.5 million in 2001, which was useful for providing enough water for irrigation purposes. Thus, the vegetation contribution was lower, and bare land contribution was higher in the year 1989 as compared to that in the year 1997. The vegetation contribution has been decreasing from the year 1997 to 2018. Urban expansion was the result of replacing bare land or vegetation with urban built-ups” (Bala et al., 2021).

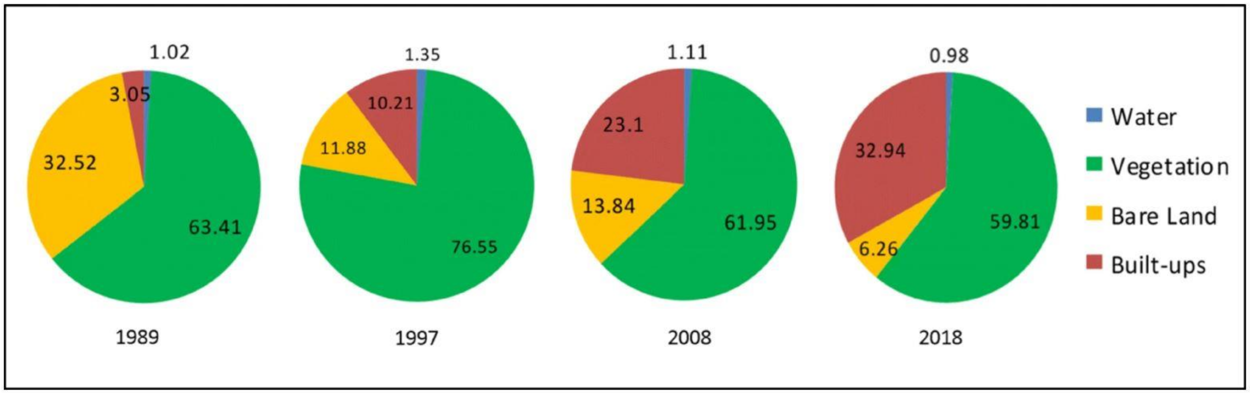

Figure 3.2 Percentage distribution of each LU/LC type (source: Bala et al., 2021)

In the built-up class of this region, the industries are also there. The river flowing through this region is highly polluted, and the significant sources of pollution are effluents discharging from the industries, sewage generated from domestic wastes, and the direct disposal of dead bodies into the river. In this region, around 200MLD (million liters per day) of domestic waste gets disposed of in the river (Kumari et al., 2021). It has been estimated that there are around 1500 industries located in and around the Varanasi region, such as the textile and leather industry, chemical industry, and metal processing industries (Mishra and Tripathi, 2008; Rai and Tripathi, 2008; Pandey et al., 2014).

3.3 Data

3.3.1 Satellite data

The essential and primary information source for this work was a series of LANDSAT-8 and LANDSAT-7 satellite images. All the images were Level 1T products, which have been precision and terrain corrected in GeoTIFF format and are in the UTM Zone 44N projection and WGS-84 as an ellipsoidal datum. The LANDSAT scenes selected for the study area were of path 142/ row43. The images have almost zero percent cloud cover and had been freely downloaded from USGS(United States Geological Survey) earth explorer website (http://earthexplorer.usgs.gov)

3.3.1.1 LANDSAT-8

There are two thermal infrared (TIR) bands in LANDSAT-8, namely, band 10 (10.60-11.9µm) and band 11 (11.50-12.51µm). The spatial resolution of TIR bands is 100m×100m, and the rest of the bands have a spatial resolution of 30m, excluding pan (band 8), which has a 15m resolution. The thermal bands have been re-sampled to 30 meters (Mukherjee et al., 2014; Sekertekin and Bonafoni, 2020; Das et al., 2021). The chosen LANDSAT scenes were between the years2013 to 2018. The impact of the stray radiance in LANDSAT 8 is more prominent for the longer wavelength band, i.e., TIRS band 11 (12.0 µm), than that in a shorter wavelength band, i.e., TIRS band 10 (10.9µm), hence steadiness of band 10 is better than band 11. Noise and stability performance for these two thermal bands are excellent, but since band 10 usually has adequate reliability performance in temperature evaluation, it should be utilized more than band 11(Montanaro et al., 2014). So, in this study, Band-10 of the LANDSAT-8 satellite has been used for the interpretation.

3.3.1.2 LANDSAT-7

LANDSAT -7 satellite comprises eight bands, including thermal and panchromatic bands. The wavelength of the thermal band lies between 10.31 to 12.36µm, and its spatial resolution is 60 meters, which is being re-sampled to 30 meters (Shukla et al., 2020; Sekertekin and Bonafoni, 2020). Band 6 is designated as a thermal band (ling et al., 2017). Thermal bands have two different kinds of gain value; one is a low gain, and the other has a high gain, but the bandwidth is the same for both gains. The high gain thermal band is used because it has greater sensitivity. The chosen LANDSAT scenes were between the years 2013 to2018.

3.3.2 Air temperature data

The air temperature data has been generated from the ERA-5 datasets. It is gridded data. The spatial resolution of this data is 0.5°×0.5°. Table 3.1 and Table 3.2 show the meteorological parameter values. The in-situ temperature datasets have been measured by using a portable thermometer. The precipitation value has been collected from the IMD (India Meteorological Department) unit in BHU (Banaras Hindu University). IMD is a government organization, and it is mainly responsible for meteorological observations, weather forecasting, and seismology. The in-situ temperature datasets have been measured by using a portable thermometer (TFX-111).

Five ERA-5 pixels cover the entire study stretch. So the median air temperature value has been given for a single day. Day 0 in tables 3.1 (A) and 3.2 (A) is the day of the satellite overpass. Day 2 and day-1are the two immediate previous days of the satellite overpass.

Table 3.1: Meteorological parameters for LANDSAT 7 images

METEOROLOGICAL PARAMETERS (Recorded at 8:30 AM)					**DATE OF IMAGE ACQUISITION**
Wind Speed (km/h)	Precipitation (in mm)			Median Air Temperature (°C)	LANDSAT 7
	2days before image acquisition	1 day before image acquisition	Day of image acquisition		
3.7	7.7	7.9	00	33.90	25 MAY 2013
00	00	00	00	19.10	1 NOV 2013
00	00	00	00	15.70	24 FEB 2015
00	00	00	00	35.70	31 MAY 2015
00	00	00	00	28.20	8 OCT 2015
00	00	00	00	14.70	13 FEB 2017
3.7	00	00	00	35.09	20 MAY 2017
3.7	00	00	00	25.80	11 OCT 2017
3.7	00	00	00	13.98	16 FEB 2018
3.7	00	00	00	35.12	8 JUNE 2018
00	00	00	00	22.20	14 OCT 2018

Day 2	Day 1	Day 0 Satellite acquisition day	
34.01°C	33.92°C	33.9°C	25-May-13
19.15°C	19.15°C	19.1°C	01-Nov-13
15.7°C	15.7°C	15.7°C	24-Feb-15
35.68°C	35.64°C	35.7°C	31-May-15
28.21°C	28.23°C	28.2°C	08-Oct-15
14.71°C	14.66°C	14.7°C	13-Feb-17
35.07°C	35.11°C	35.09°C	20-May-17
25.84°C	25.82°C	25.8°C	11-Oct-17
13.97°C	14.02°C	13.98°C	16-Feb-18
22.24°C	22.23°C	22.2°C	14-Oct-18

Table 3.1 (A)

Table 3.2: Meteorological parameters for LANDSAT 8 images

METEOROLOGICAL PARAMETERS (Recorded at 8:30 AM)					**DATE OF IMAGE ACQUISITION**
Wind Speed (km/h)	Precipitation (mm)			Median Air Temperature (°C)	LANDSAT 8
	2days before image acquisition	1 day before image acquisition	Day of image acquisition		
3.7	00	00	00	30.70	1 MAY 2013
5.56	00	00	00	21.36	24 OCT 2013
3.7	00	00	00	14.4	1 FEB 2015
3.7	3.9	3.8	00	32.5	24 JUNE 2015
00	00	00	00	19.50	15 NOV 2015
00	00	00	00	13.88	21 FEB 2017
5.56	2.6	2.4	00	32.14	29 JUNE 2017
00	00	00	00	20.23	4 NOV 2017
00	00	00	00	17.58	24 FEB 2018
3.7	12.1	8.7	00	29.1	15 MAY 2018
00	00	00	00	23.3	22 OCT 2018

Table 3.2 (A)

Day 2	Day 1	Day 0 Satellite acquisition day	
30.68°C	30.68°C	30.7°C	01-May-13
21.37°C	21.35°C	21.36°C	24-Oct-13
14.42°C	14.44°C	14.4°C	01-Feb-15
32.5°C	32.5°C	32.5°C	24-Jun-15
19.42°C	19.42°C	19.5°C	15-Nov-15
13.83°C	13.95°C	13.88°C	21-Feb-17
32.14°C	32.04°C	32.14°C	29-Jun-17
20.31°C	20.32°C	20.23°C	04-Nov-17
17.64°C	17.59°C	17.58°C	24-Feb-18
29.12°C	29.09°C	29.1°C	15-May-18
23.41°C	23.29°C	23.3°C	22-Oct-18

3.4 Methodology

The methodology described here is for calculating the water surface temperature from LANDSAT 8 and LANDSAT 7 Thermal Infrared (TIR) images. In the present work, the thermal pattern of the river Ganga has been studied for the stretch situated between Mirzapur and Ghazipur. The analysis has been done with LANDSAT-8 and LANDSAT-7 satellite images. The steps are shown in Figure 3.5 for LANDSAT-8 satellite image analysis. For the LANDSAT-7, image analysis steps are similar with just minor modifications. Band 2,4 has been used for LANDSAT-7 to make Normalized Difference Water Index (NDWI), and Band 6 TIR has been used for temperature evaluation.

3.4.1 Atmospheric correction

The thermal bands of the satellites are affected by atmospheric effects. These effects will induce noise in the radiance signal, which, in turn, can cause computational error. So to remove these errors, we have to do atmospheric correction so that it can minimize the atmospheric effects. For the corrected water surface radiance, several atmospheric parameters like $L_{\lambda up}$(upwelling radiance), τ(atmospheric transmissivity), $L_{\lambda d}$(downwelling radiance) will be required. Also, in addition to these parameters ‘ε’ (water emissivity) value will also be needed. Atmospheric parameters ($L_{\lambda up}$, τ, $L_{\lambda d}$) were obtained from the ‘Atmosphere Correction Parameter Calculator’(https://atmcorr.gsfc.nasa.gov/) (Lamaro et al. 2013; Ling et al., 2017). In the present work, the emissivity of water was taken as 0.9885 (Ling et al., 2017).

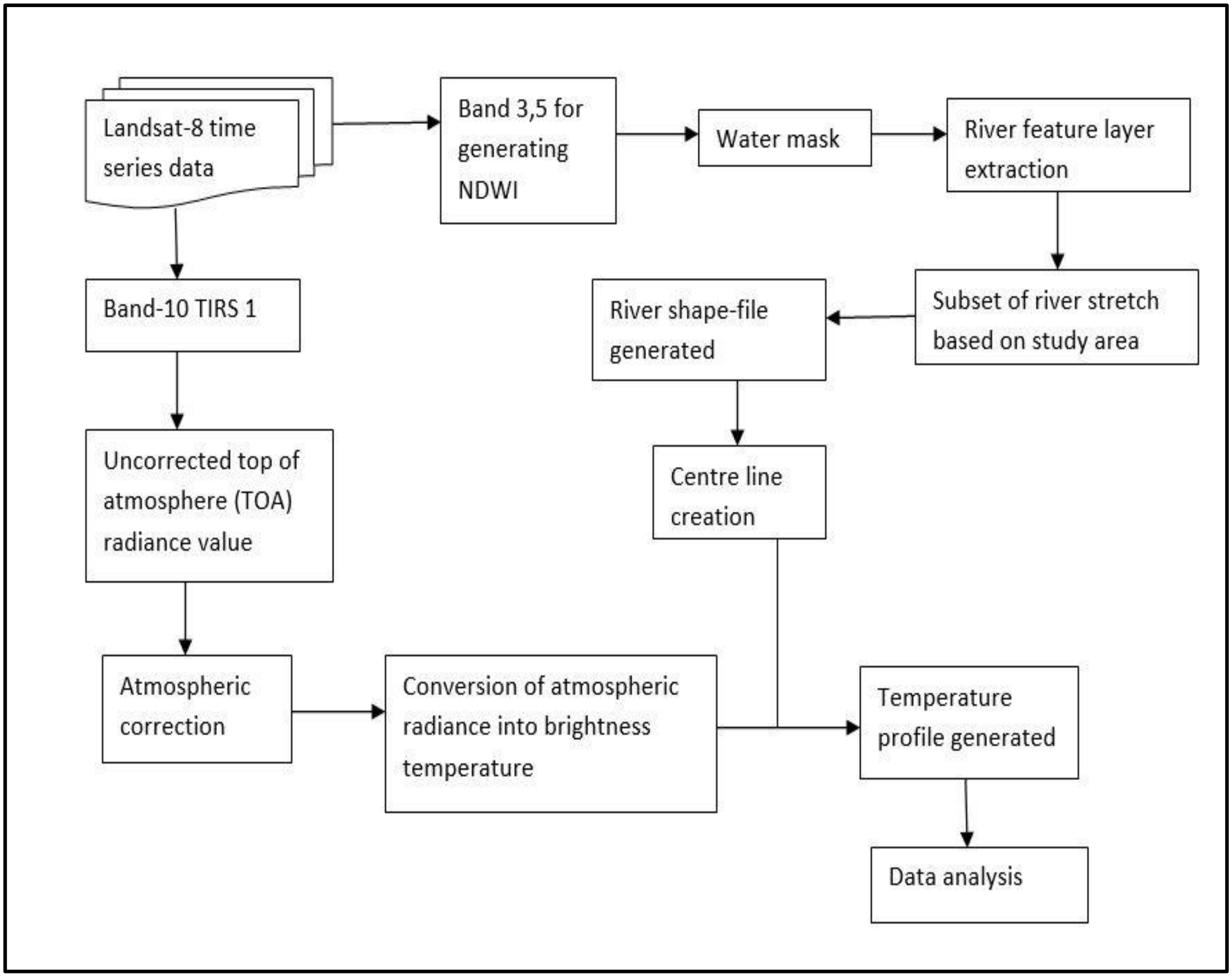

Figure 3.3 Flowchart of the methodology for temperature estimation from L8

3.4.2 Creating the water mask

NDWI (Normalized Difference Water Index) was used to create the water mask. NDWI was computed from NIR and Green bands, each with 30m spatial resolution, and pixels with a threshold of 0.5 and above were converted to the polygon. The river boundary was then selected from the attribute table and exported as a separate shapefile in Arc Map 10.5. The shapefile was then used to clip the river from the TIR band numbers 6 and 10 of LANDSAT-7 and LANDSAT-8, respectively. (Gautam et al., 2015; Sarp and Ozcelik, 2017). NDWI is calculated according to the following formula:

$$NDWI = \frac{(\mathrm{GREEN} - \mathrm{NIR})}{(\mathrm{GREEN} + \mathrm{NIR})} \tag{3.1}$$

After calculating the NDWI value, pixels containing water bodies will be highlighted. This processed image was then used to delineate the river boundary in the study area, and its shapefile was created. This shapefile was then used to prepare the thermal images in Arc GIS. At the same time, the river boundary was further contracted by excluding three inhomogeneous thermal pixels from each side of the river to exclude the overlap of terrestrial signals. Moreover, only one pixel on either side of the central line of the river was considered for the spatio-temporal analysis of surface water temperature (SWT), thus completely avoiding the intrusion of any inhomogeneous pixel.

3.4.3 Surface water temperature calculation

For calculating the surface water temperature, specific features of LANDSAT-8 and LANDSAT-7 have been delineated in the following sections.

3.4.3.1 LANDSAT-8

For the estimation of the surface temperature of river water, Top of Atmosphere (TOA) spectral radiance needs to be calculated first, using the formula:

$$L_\lambda = M_L * Q_{cal} + A_L \tag{3.2}$$

where L_λ is the TOA spectral radiance (Watts/(m^2*srad*μm)), M_L is Band-Specific Multiplicative re-scaling factor from metadata, Q_{cal} is quantized, and calibrated standard product pixel value DN, and A_L is Band-Specific additive re-scaling factor from metadata. Afterward, the calculated TOA value is corrected by using the formula:

$$L_{\lambda cor}=\tau.\varepsilon.L_\lambda+ L_{\lambda up}+ L_{\lambda d}(1-\varepsilon).\tau \tag{3.3}$$

where symbols have the usual meanings as described in the *atmospheric correction* section (Section 3.4.1). Then, with the use of formula number 3.4 we can convert the spectral radiance into temperature in degree Celsius:

$$T= [K_2 /(\ln((K_1 /L_{\lambda cor})+1))]-273.15 \tag{3.4}$$

where K_1 and K_2 are the thermal constants of the satellite (Barsi et al., 2014; Rajeshwari and Mani, 2014). M_L and A_L values for the required area of interest are 0.000342 and 0.1, respectively. K1 and K2 values of the LANDSAT-8 satellite's TIR band-10 for the area of interest are 774.8853 and 1321.0789, respectively. The values of all these parameters can be found in satellite imagery's metadata file, which is downloaded along with the satellite imagery (Rajeshwari and Mani, 2014). The atmospheric correction has been done by using the atmospheric correction calculator developed by NASA (Barsi et al., 2003). The final temperature is the value of the target. In this case, it will be river temperature.

3.4.3.2 LANDSAT-7

For calculating the TOA radiance same formula (i.e., equation 3.2) has been used. The additive and multiplicative scale factors are different in this case. The M_L value is 0.0372, and A_L is 3.16 (LANDSAT-7 metadata). Further, the TOA value is converted to a surface leaving radiance by taking into account the target emissivity (in this case, the emissivity of water has been taken). This step eliminates the effect of the atmosphere, which is the essential aspect for the calculation of the temperature based on the radiative transfer function(Ling et al., 2017). The equation is:

$$L_{\lambda(Ts)}=[\{(L_{\lambda}-L_{\lambda up})/(\tau\times\varepsilon)\}-\{((1-\varepsilon)/\varepsilon)\times L_{\lambda d})] \qquad (3.5)$$

$\mathbf{L_{\lambda(Ts)}}$ is the corrected surface radiance. The rest of the parameters are already mentioned in section 3.4.1

Finally, the corrected water surface radiance was converted to water temperature using a sensor-specific approximation of Planck's equation (Chander and Markham, 2003). The formula for this approximation is :

$$T_s=[K_2\times[\ln(K_1/(L_{\lambda(Ts)}+1))]-1]-273.15 \qquad (3.6)$$

T_s is the surface water temperature in °C. K_1 and K_2 are the thermal constants of the ETM+ sensor where K_1 is 1282.71 Kelvin and K_2 is 666.09 $W.m^2.sr.mm$

3.5 Results

3.5.1 Estimated Water Temperature

The validation process was performed by comparing the water temperature values obtained through a portable thermometer and the surface water temperature calculated from the satellite images. For the LANDSAT-8 satellite, two images had been taken for validation purposes. Images for LANDSAT-8 are of 24th January 2018 and 8th February 2018. For L7, the image of

20th May 2017 has been chosen. For the LANDSAT-7 overpass, the Varanasi region's in-situ sampling was done on 21st May 2017. In-situ data were recorded for several points within the study stretch. A total of, 30 points were selected for validation of one type of satellite image. Thirty points are recorded for the L7 images. Similarly, thirty in-situ points have been recorded for L-8 images as well. Fifteen points were chosen on a particular day because the time frame for recording in-situ points temperature had been fixed and done from 9:45 AM IST to 11:00 AM IST. This small time frame has been chosen because the satellite specifically passes at around 10:20 AM IST, and if we start to record in-situ temperature from a time way before the overpass to a time way after the overpass, then there is a possibility that in-situ temperatures may have fluctuated much more with respect to satellite estimated temperature and the more error-prone result will be observed for validation. During this small-time frame, temperature for only15 points can be measured in the study stretch. The sampling points and their location, along with the dates of in-situ sampling, are given in Figure 3.4, Figure 3.5, Figure 3.6, and Figure 3.7. All these points are situated approximately in the mid-section of the river Ganga. To mark the coordinates of the points, “Garmin Etrex 30” GPS was used.

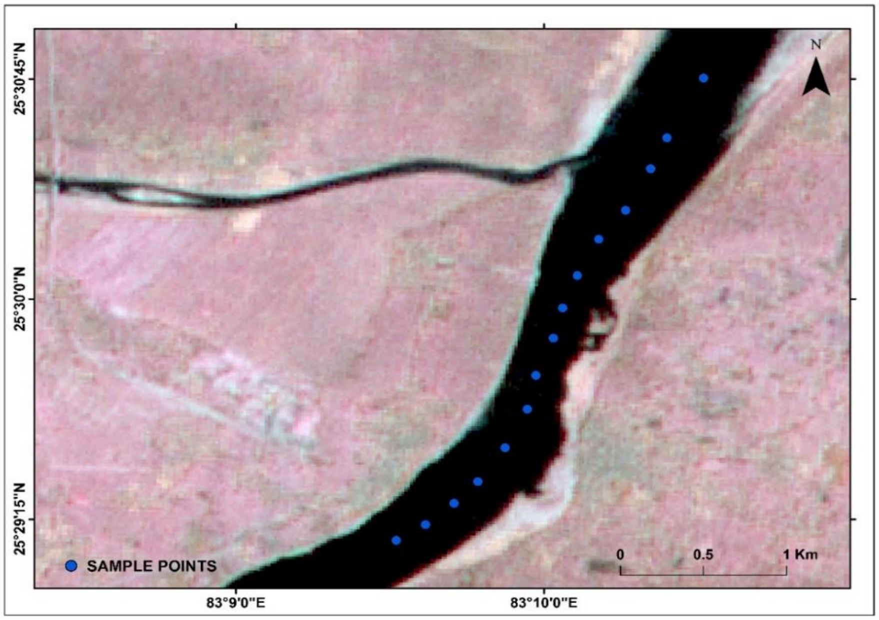

Figure 3.4 Sampling point for Ghazipur (LANDSAT-7 overpass; date 20th May, 2017)

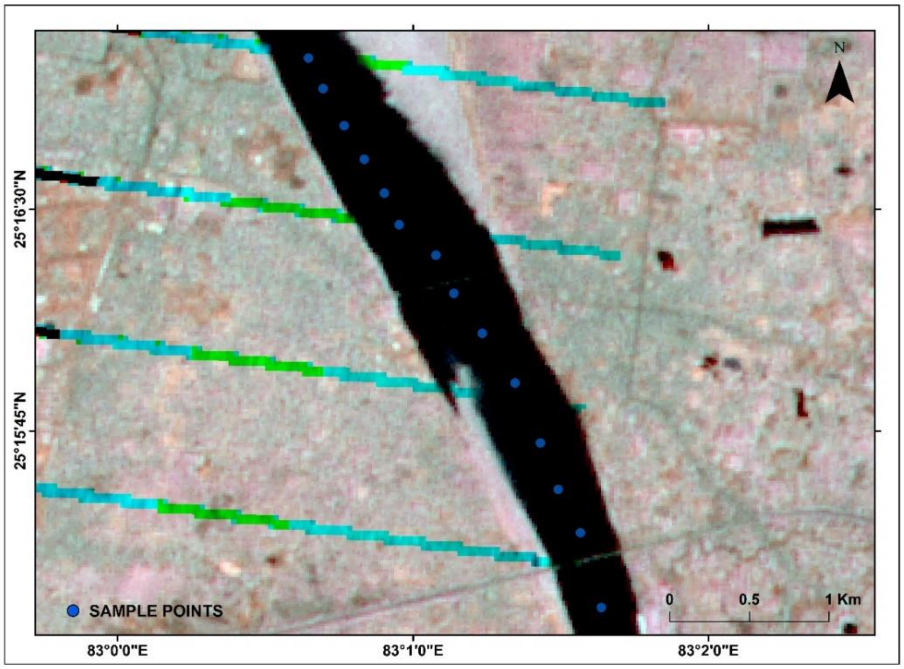

Figure 3.5 Sampling point for Varanasi (LANDSAT-7 overpass; date 20th May, 2017)

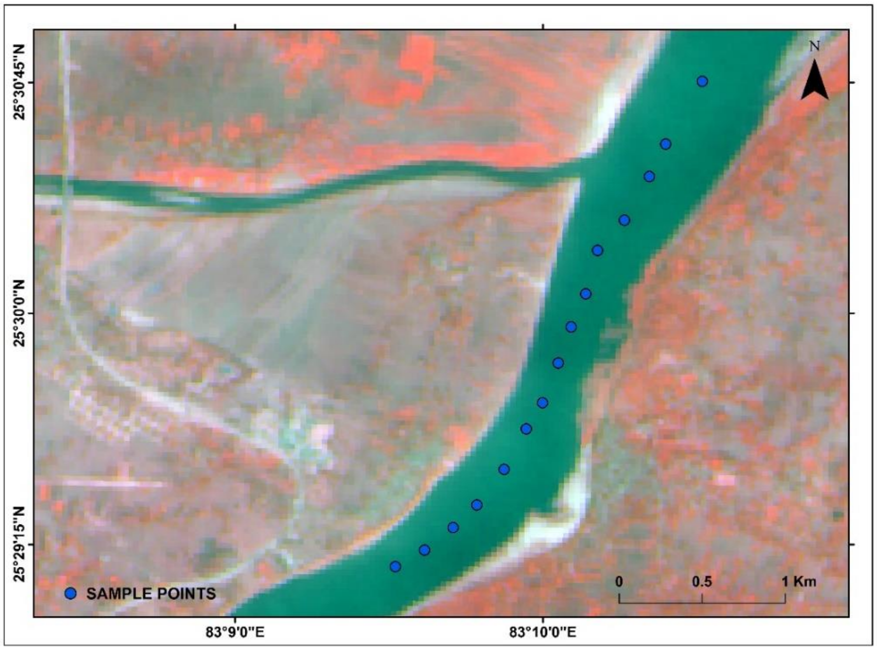

Figure 3.6 Sampling point for Ghazipur (LANDSAT-8 overpass; date 24th January, 2018)

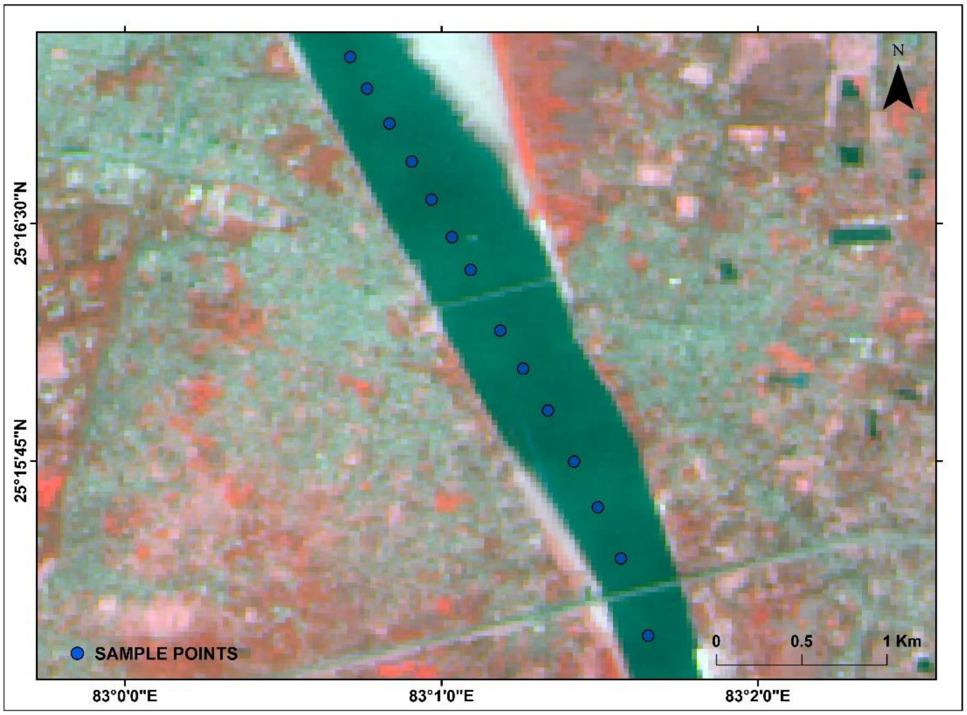

Figure 3.7 Sampling point for Varanasi (LANDSAT-8 overpass; date 8th February, 2018)

Figure 3.8 Field photographs while doing the in-situ sampling

Figures 3.9 and 3.10 show the regression plots between the temperature calculated from satellite images and the temperature recorded by the portable thermometer. Correlation for L8 estimated temperature with the portable thermometer is better in comparison to L7 estimated temperature. The Root Mean Square Error (RMSE) value is more for the temperature calculated from L7 satellite imageries. Thus, it can be said that the temperature estimation from LANDSAT7 will be somewhat less accurate in comparison to LANDSAT8 temperature estimation.

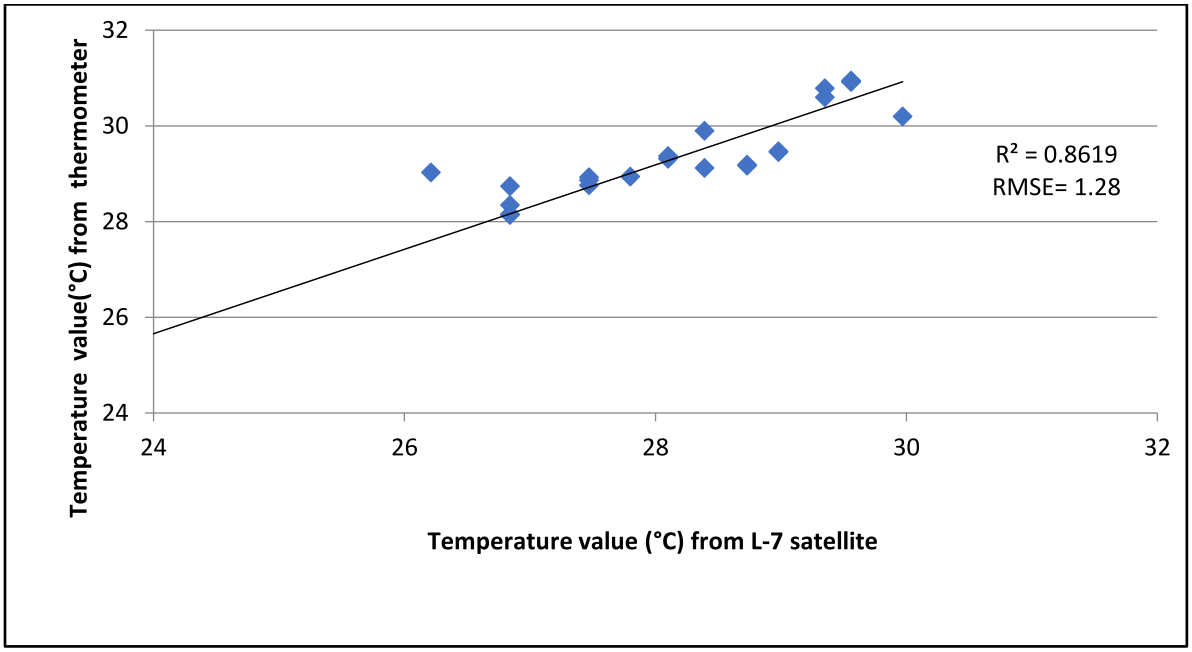

Figure 3.9 Regression plot for the LANDSAT-7 and in-situ temperature

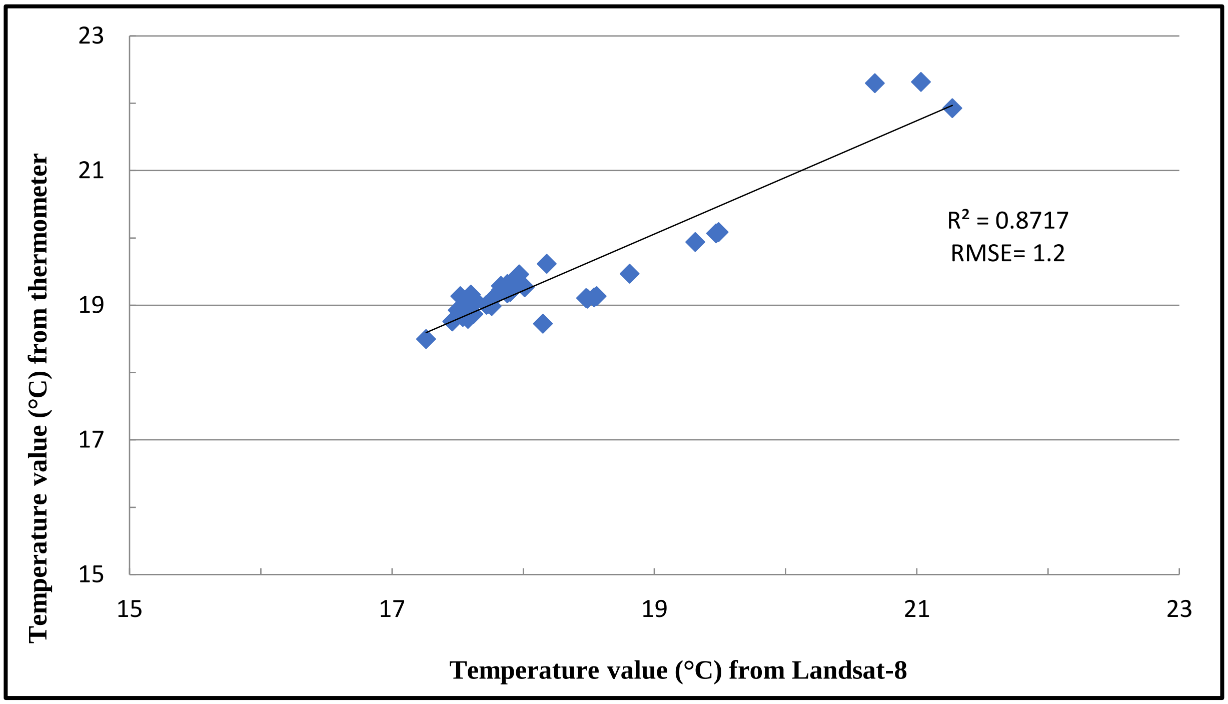

Figure 3.10 Regression plot for the LANDSAT-8 and in-situ temperature

3.5.2 Temporal and longitudinal variation of river thermal profile

The thermal profile calculated from LANDSAT-7 and LANDSAT-8 images has been described below.

3.5.2.1 Thermal profile calculated from LANDSAT-7 images

The river's temporal thermal profile's box plot has been represented in Figures 3.11, 3.12, and 3.13. This is a combined box plot for the estimated temperature of LANDSAT-7 and LANDSAT-8 satellite thermal images. The time period, which is under consideration, is from 2013 to 2018.

For LANDSAT-7 thermal images, three seasons were chosen for a year to analyze the temporal variation, namely the spring and winter (February), summer (May-June), and autumn/pre-winter season (October-November). The third season of autumn and pre-winter can also be called the post-monsoon time period in the context of the Indian climate. In the summer season for some of the years' May has been selected and June for others. This has been done to avoid cloud cover in images. A similar scenario happens for the autumn and pre-winter season, so two months, i.e., October and November, have been taken into account.

The overall median temperature for February is the lowest among all the selected time periods. If the comparison can be made among the years of February, then it can be interpreted that February 2015 had the highest median temperature among all.

As usual, the summer season surface water temperature is higher than the other two seasons for the respective years. The month of May-2013 had shown a dip in the temperature as compared to other year’s May months, and this had because of unseasonal precipitation that happened at that time. For the month of June-2018, the water temperature values are erroneous because this imagery consists of cloud cover. For the year 2018, during the summer period of May–June, unfortunately, no cloud-free images were available for the study stretch, so this image of June-2018 has been chosen, which has the least cloud cover among all other available summertime L7 images of 2018 for the study area. For the autumn/pre-winter season, the November 2013 temperature is the lowest, and the temperature for the month of October is lying in the range of 25-27°C. All the images that were acquired for the month of October were dated between the first and fifteen October, so the October month temperatures were lying in that range.

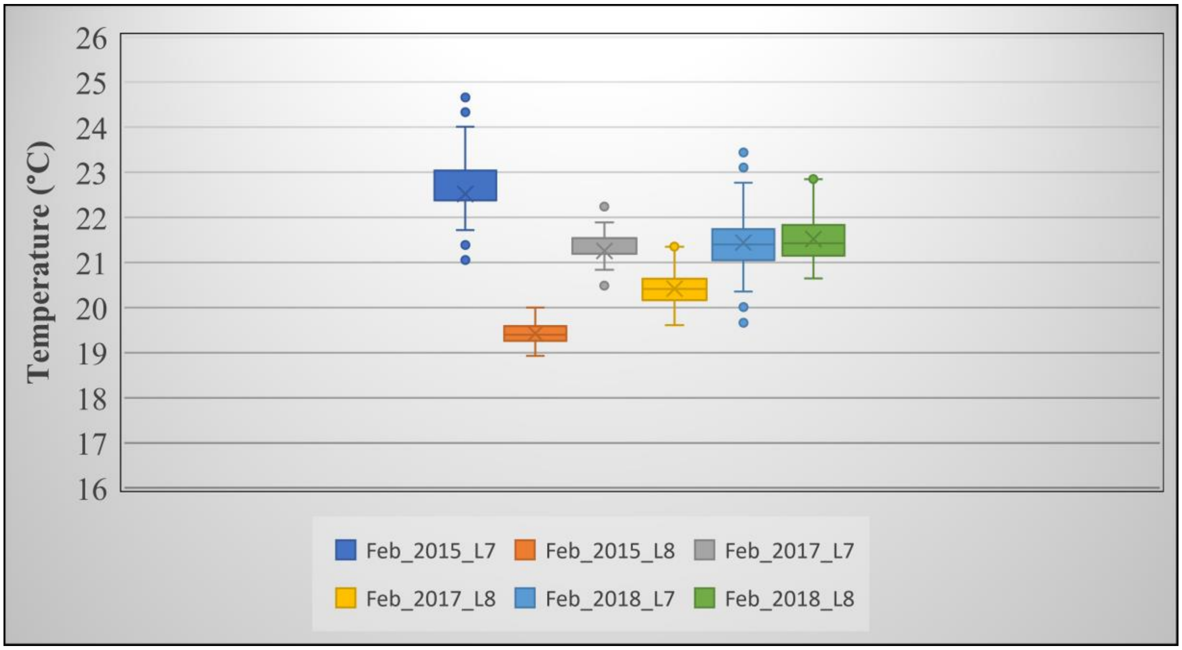

Figure 3.11 Temporal thermal box plot for the month of February for LANDSAT-7 and LANDSAT-8

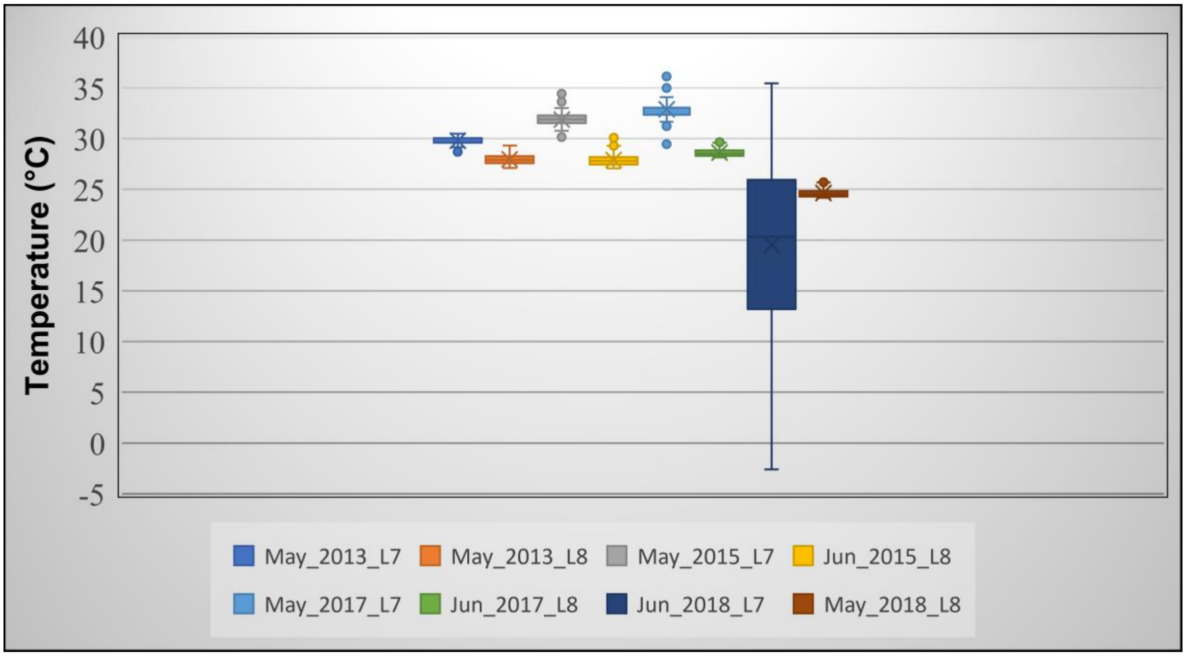

Figure 3.12 Temporal thermal box plot for the month of May-June for LANDSAT-7 and LANDSAT-8

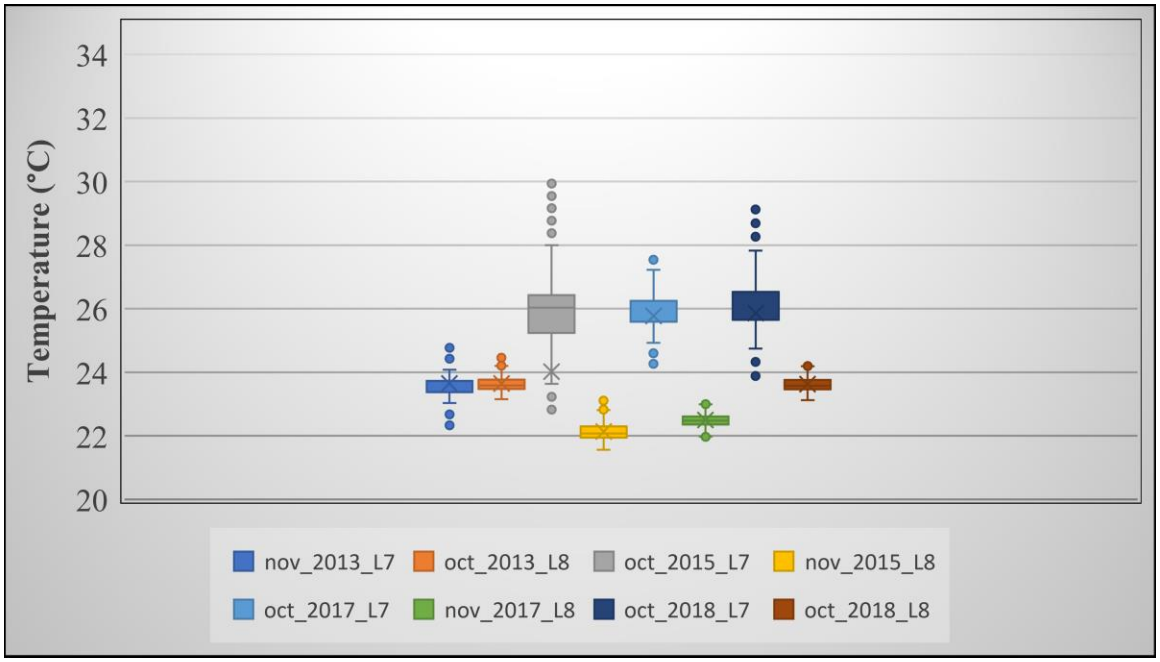

Figure 3.13 Temporal thermal box plot for the month of October-November for LANDSAT-7 and LANDSAT-8

The longitudinal temperature profile of the river for the study stretch had been calculated from the L7 satellite imagery. It was shown in Figures 3.14, 3.15, 3.16, 3.17, 3.18, 3.19, 3.20, 3.21, 3.22, and 3.23**.** Temperature values are in degrees Celsius, and those values are plotted in the y-axis of the graph. Data gaps can be observed in those graphs because LANDSAT-7 satellite images have scan line errors.

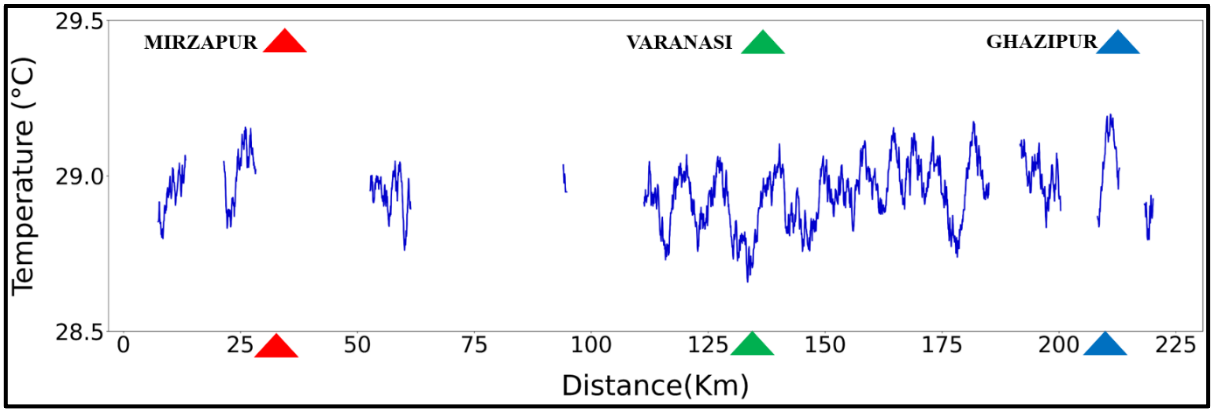

Figure 3.14 Spatial thermal profile for May 2013

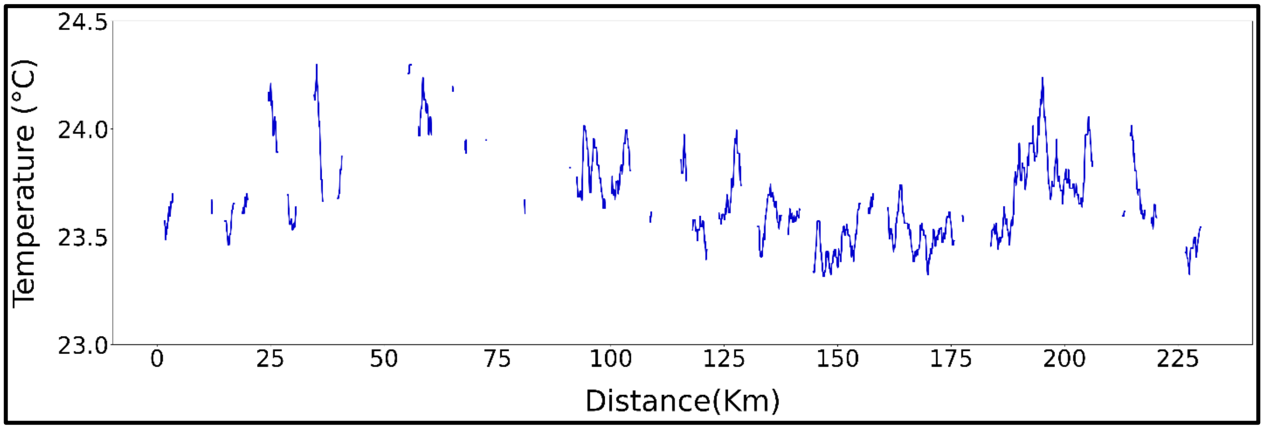

Figure 3.15 Spatial thermal profile for November 2013

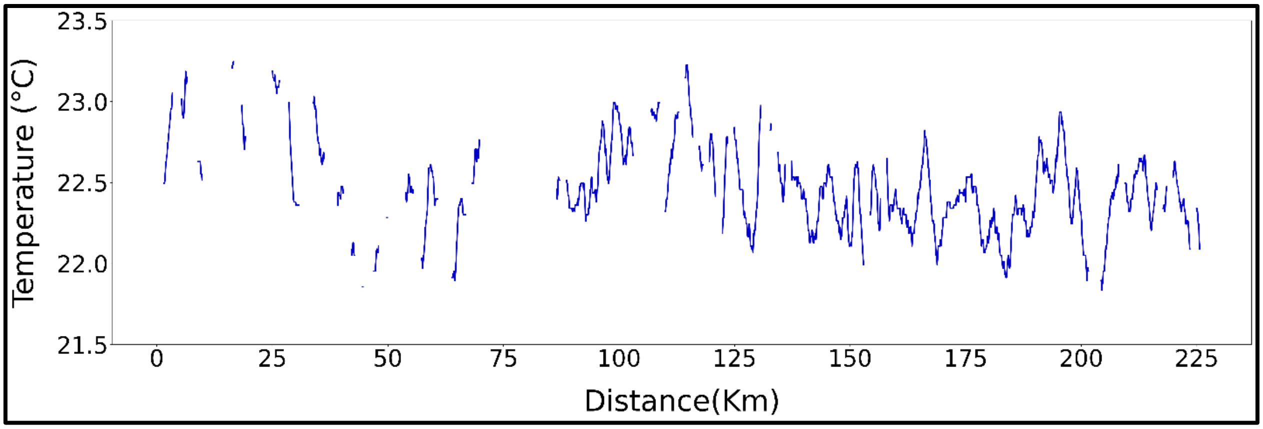

Figure 3.16 Spatial thermal profile for February 2015

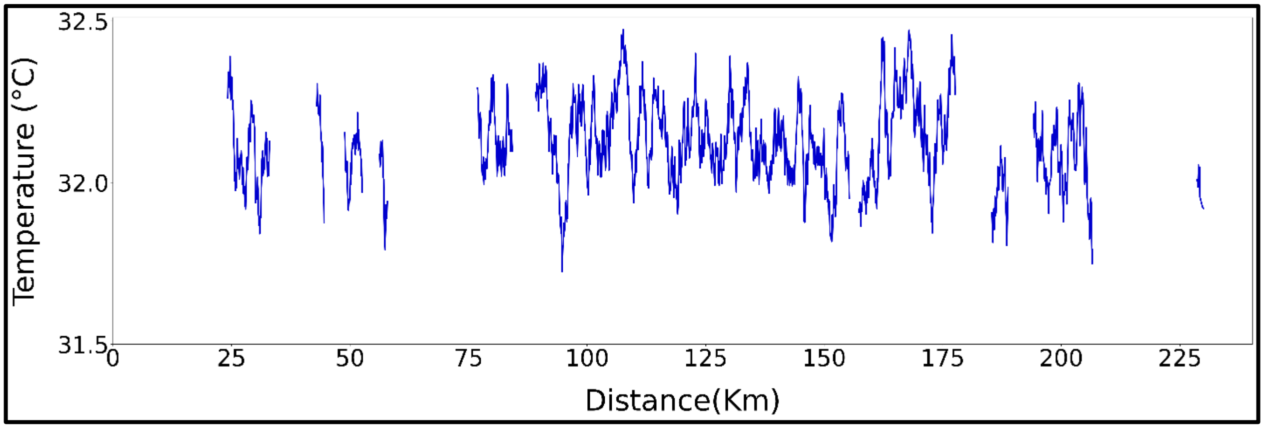

Figure 3.17 Spatial thermal profile for May 2015

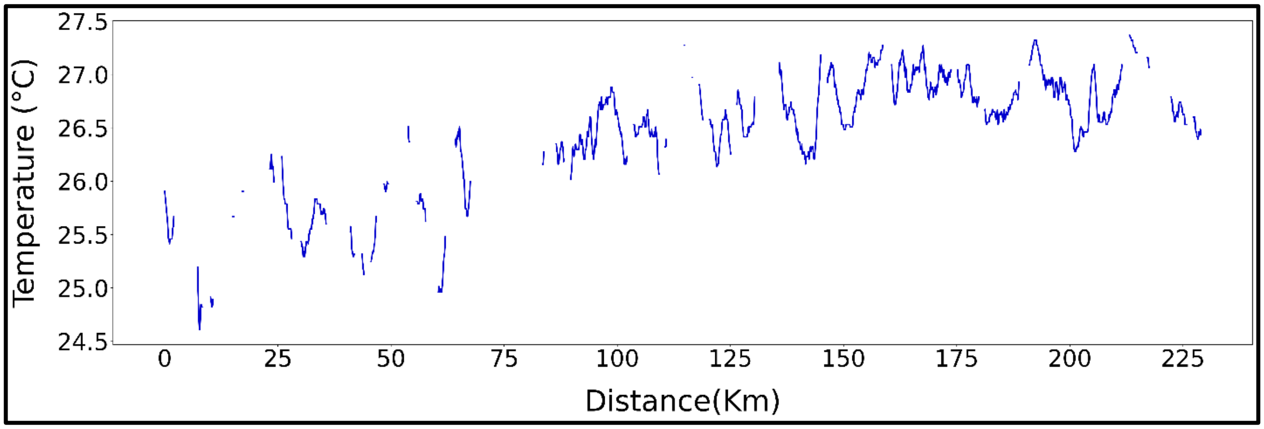

Figure 3.18 Spatial thermal profile for October 2015

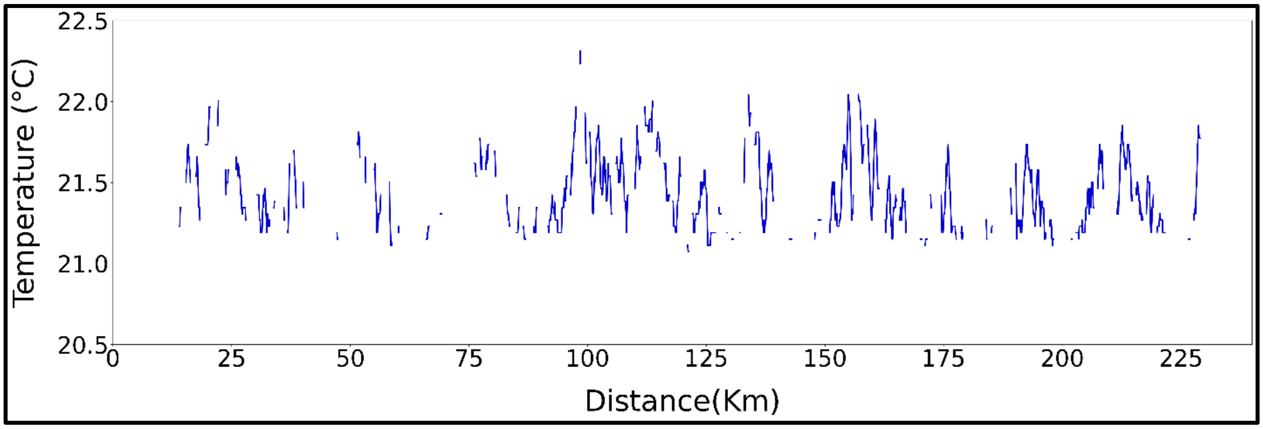

Figure 3.19 Spatial thermal profile for February 2017

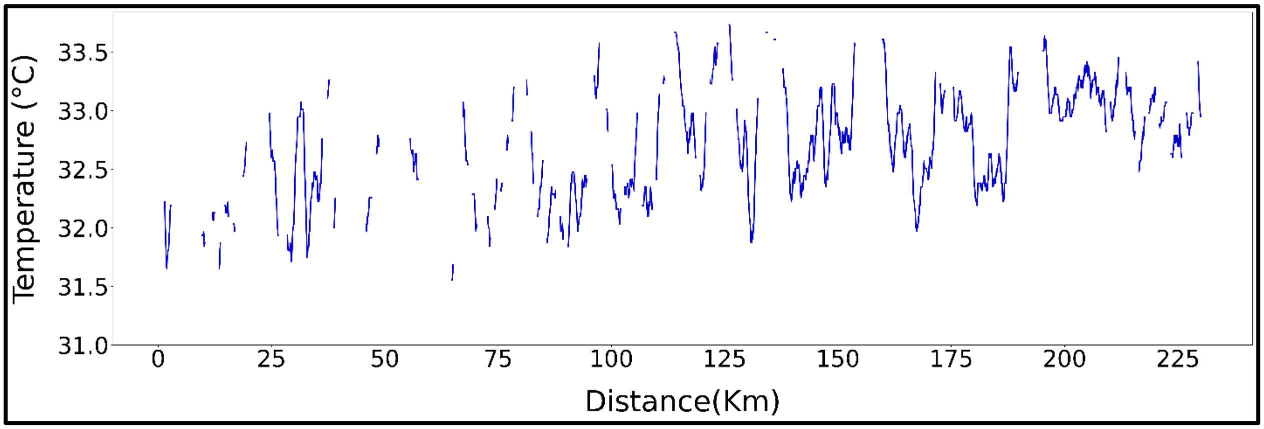

Figure 3.20 Spatial thermal profile for May 2017

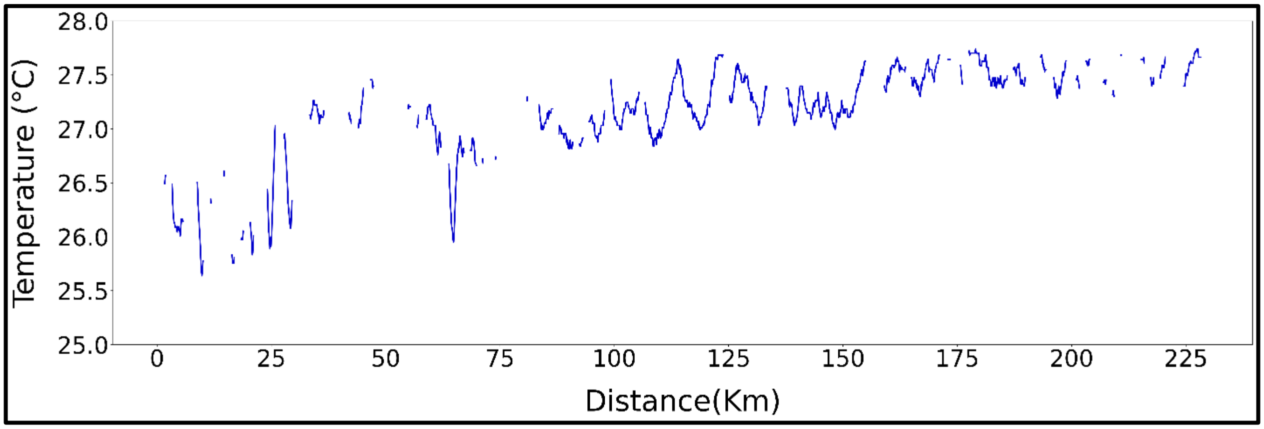

Figure 3.21 Spatial thermal profile for October 2017

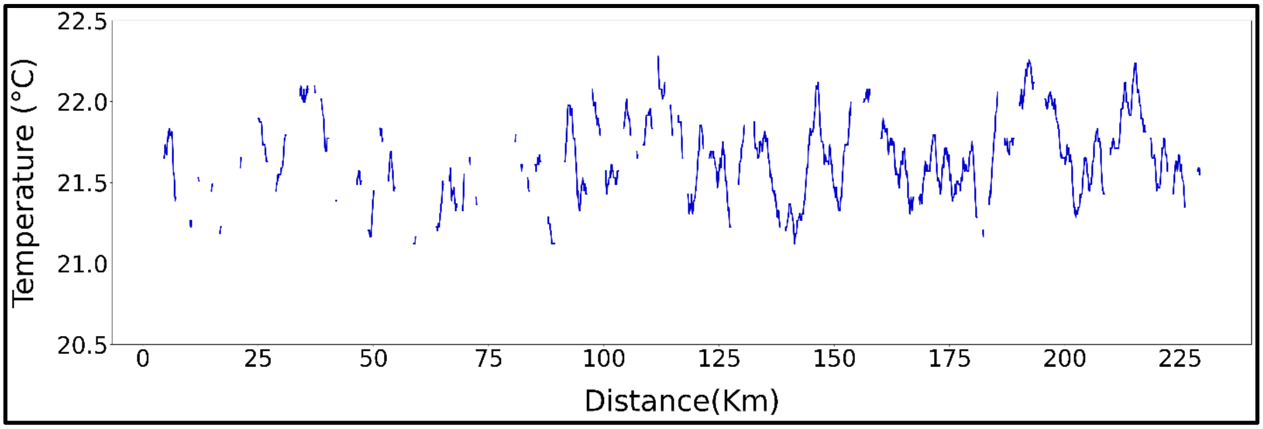

Figure 3.22 Spatial thermal profile for February 2018

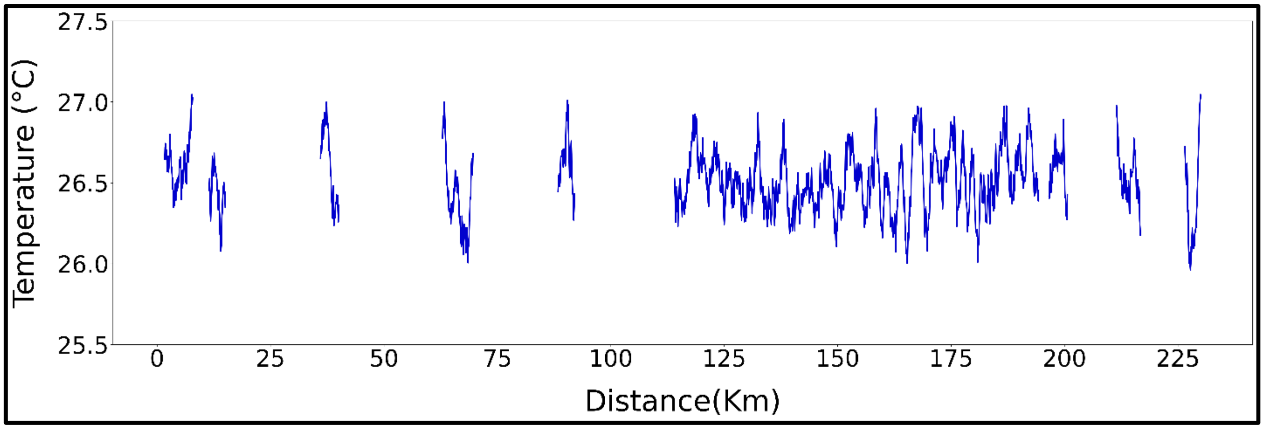

Figure 3.23 Spatial thermal profile for October 2018

3.5.2.2 Thermal profile calculated from LANDSAT-8 images

For the summer period, which consists of May or June month, it can be seen that May-2018 has the lowest median temperature because during that time, precipitation had happened in the region, and the air temperature was also quite low as compared to any other normal day of May month. The precipitation during May month is quite unnatural in this region. South-west monsoon generally arrives in northern India in the first week of July. The two images of June month were acquired during the period of pre-monsoon, and during this time, some scattered precipitation occurred in this region, so the stream temperature of the June images was quite low.

The post-monsoon and pre-winter time period has been depicted with the month of October or November. The temperature of October is higher than that of November, which is quite evident because, from November, the onset of winter starts in the northern regions of India.

Figures 3.24, 3.25, 3.26, 3.27, 3.28, 3.29, 3.30, 3.31, 3.32, 3.33, and 3.34 show a longitudinal profile graph for L8 satellite calculated temperature. There are no data gaps in these figures as there is no problem with scan line error in the LANDSAT-8 satellite sensor system.

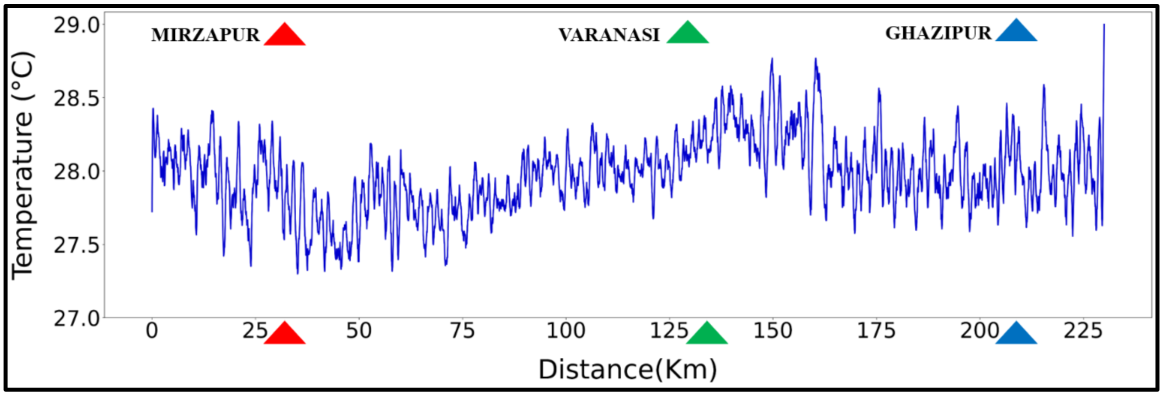

Figure 3.24 Spatial thermal profile for May 2013

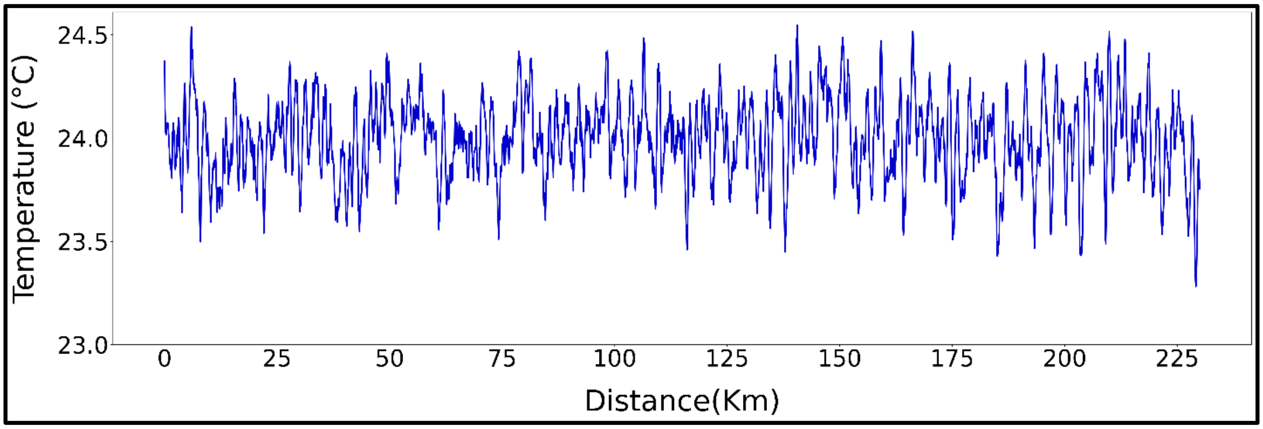

Figure 3.25 Spatial thermal profile for October 2013

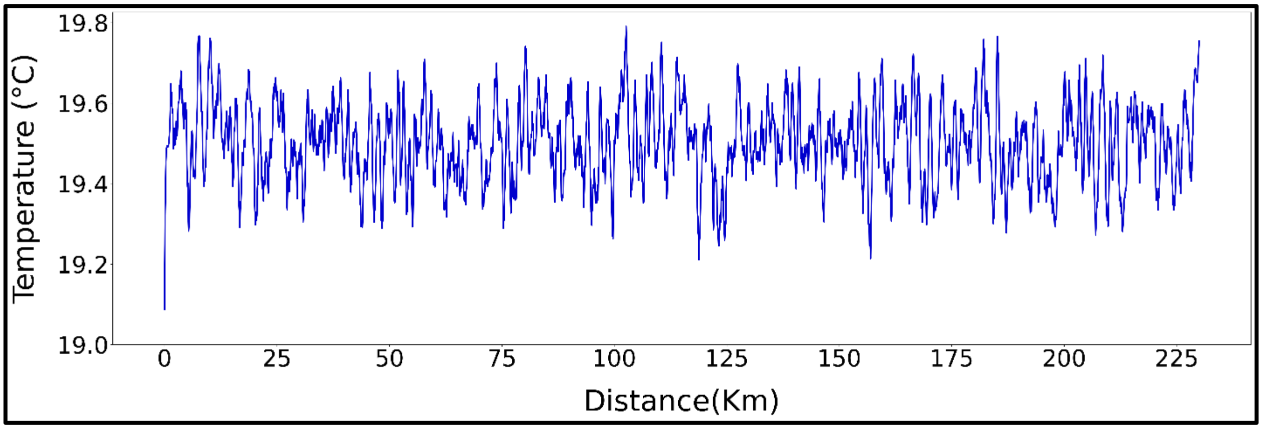

Figure 3.26 Spatial thermal profile for February 2015

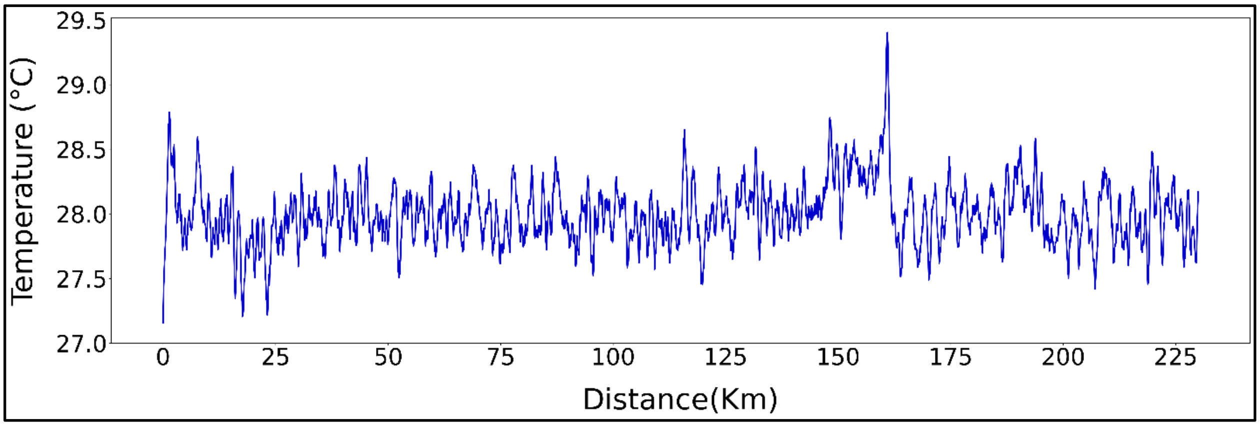

Figure 3.27 Spatial thermal profile for June 2015

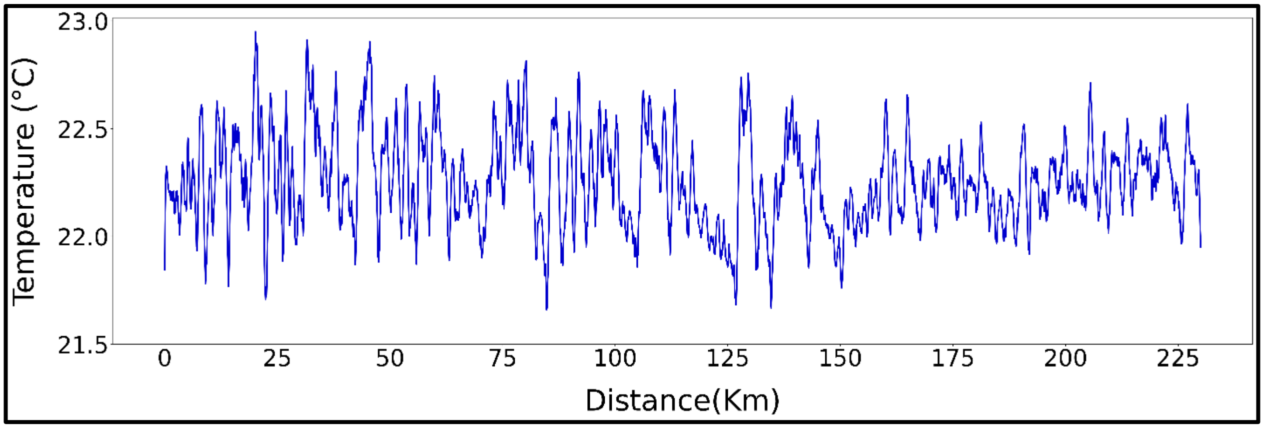

Figure 3.28 Spatial thermal profile for November 2015

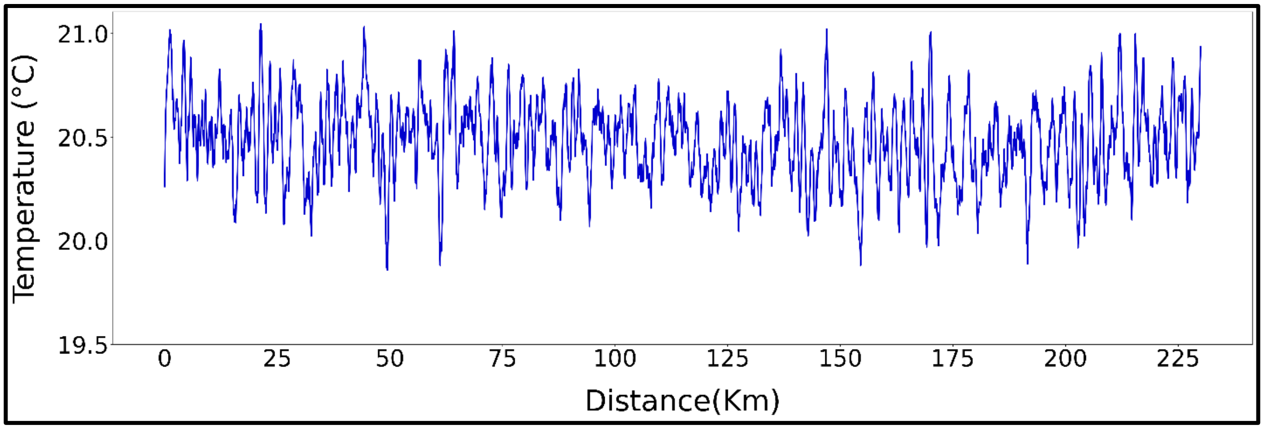

Figure 3.29 Spatial thermal profile for February 2017

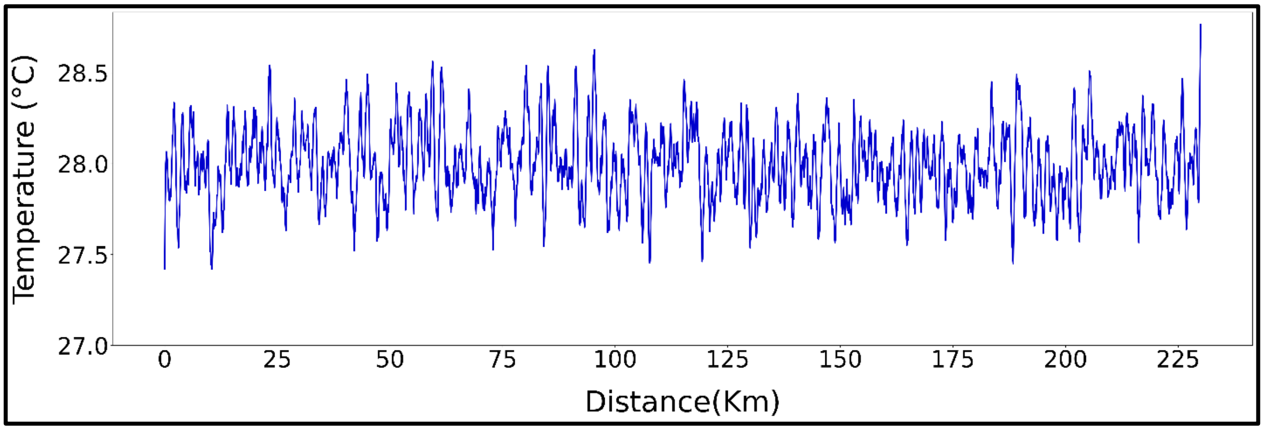

Figure 3.30 Spatial thermal profile for June 2017

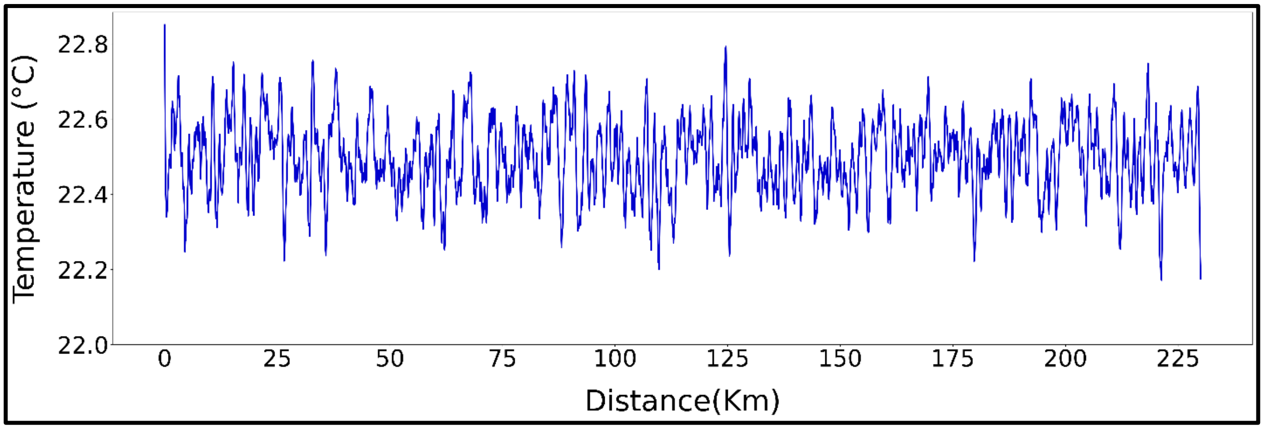

Figure 3.31 Spatial thermal profile for November 2017

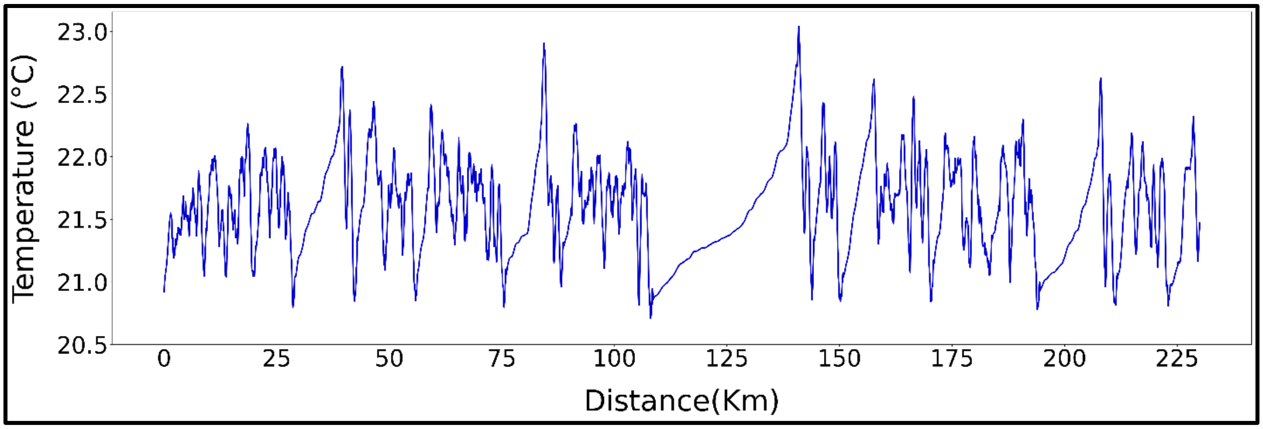

Figure 3.32 Spatial thermal profile for February 2018

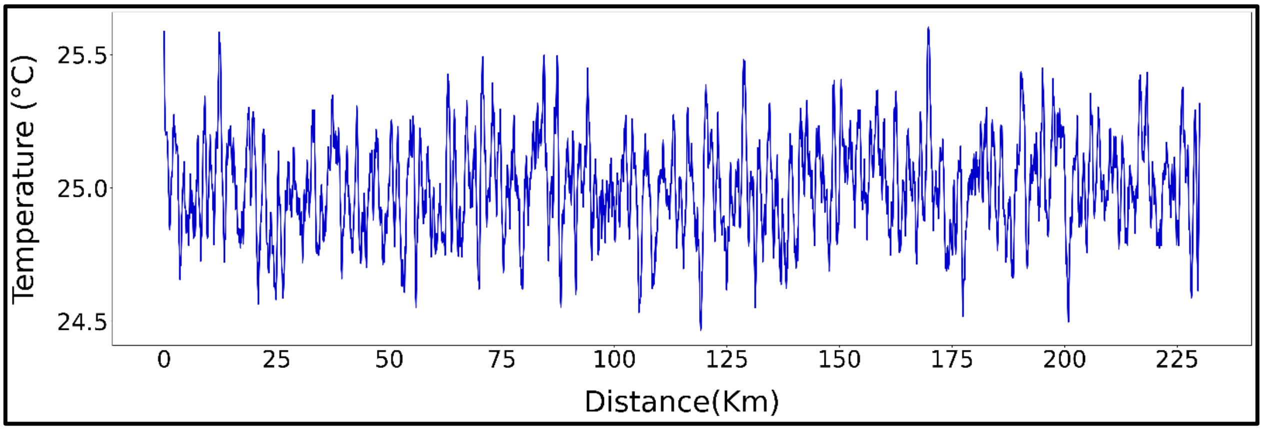

Figure 3.33 Spatial thermal profile for May 2018

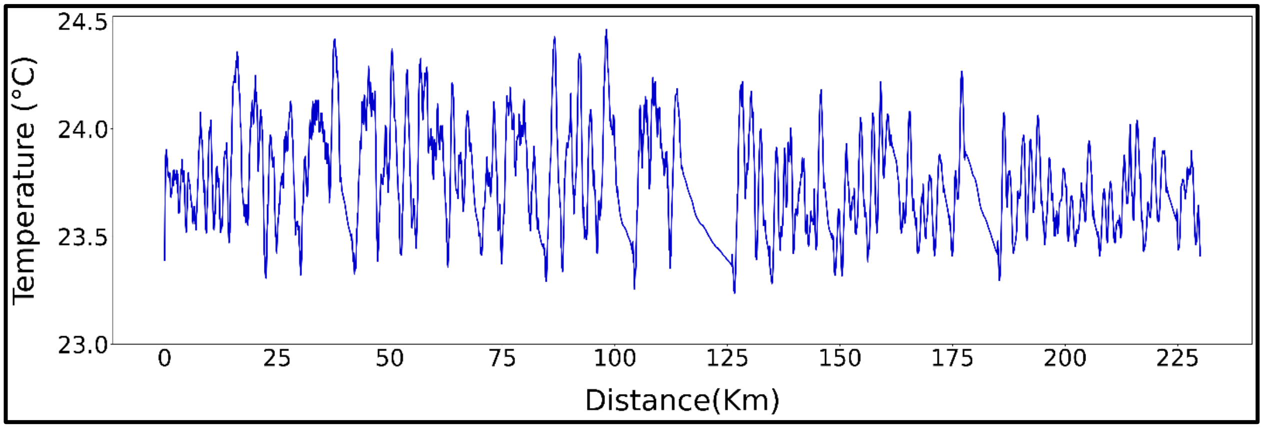

Figure 3.34 Spatial thermal profile for October 2018

3.5.3 Relationship between air temperature, LANDSAT-7&8 satellite calculated temperature

From Table 3.3, it can be seen that air temperature shows a better relationship with LANDSAT-8 satellite estimated surface water temperature in comparison to the LANDSAT-7 satellite estimated temperature. For February, three year's data have been taken, i.e., 2015, 2017, and 2018. Similarly, for the May-June and October-November, four year's data have been taken, i.e., 2013, 2015, 2017, and 2018. Air temperature values that are observed from ERA-5 datasets.

Table 3.3: Relationship between Air temp. and L8, L7 satellite water surface estimated temp.

Months	**L8**	**L7**
February	0.70	0.68
May-June	0.75	0.73
October-November	0.71	0.69

The correlation plots (R^2) have been given for each of the L8 and L7 satellites. The season-wise correlation plot has been depicted. The median temperature for both the air and water was calculated for each satellite overpass day, and then it was plotted. The reason for estimating the median is that the spatial resolution for LANDSAT series satellite and ERA-5 datasets are entirely different.

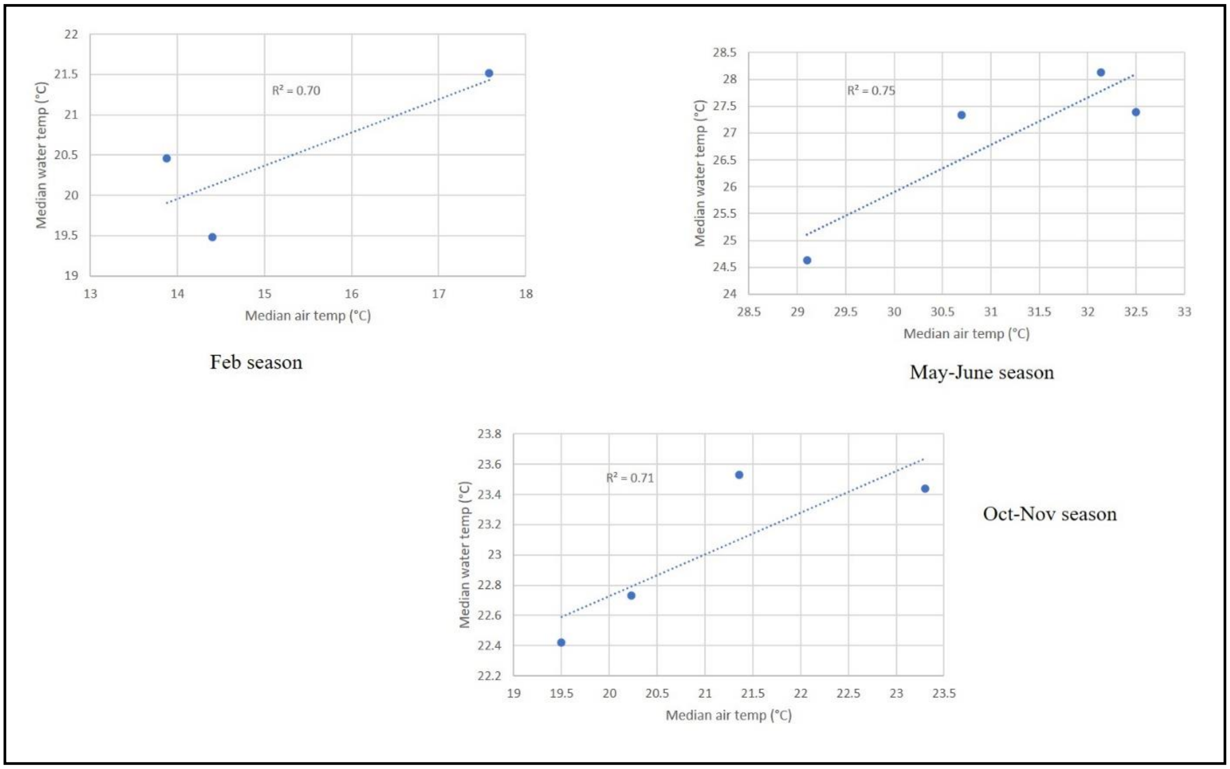

Figure 3.35 Season-wise meadin air temp and water surface temp for L-8 datasets

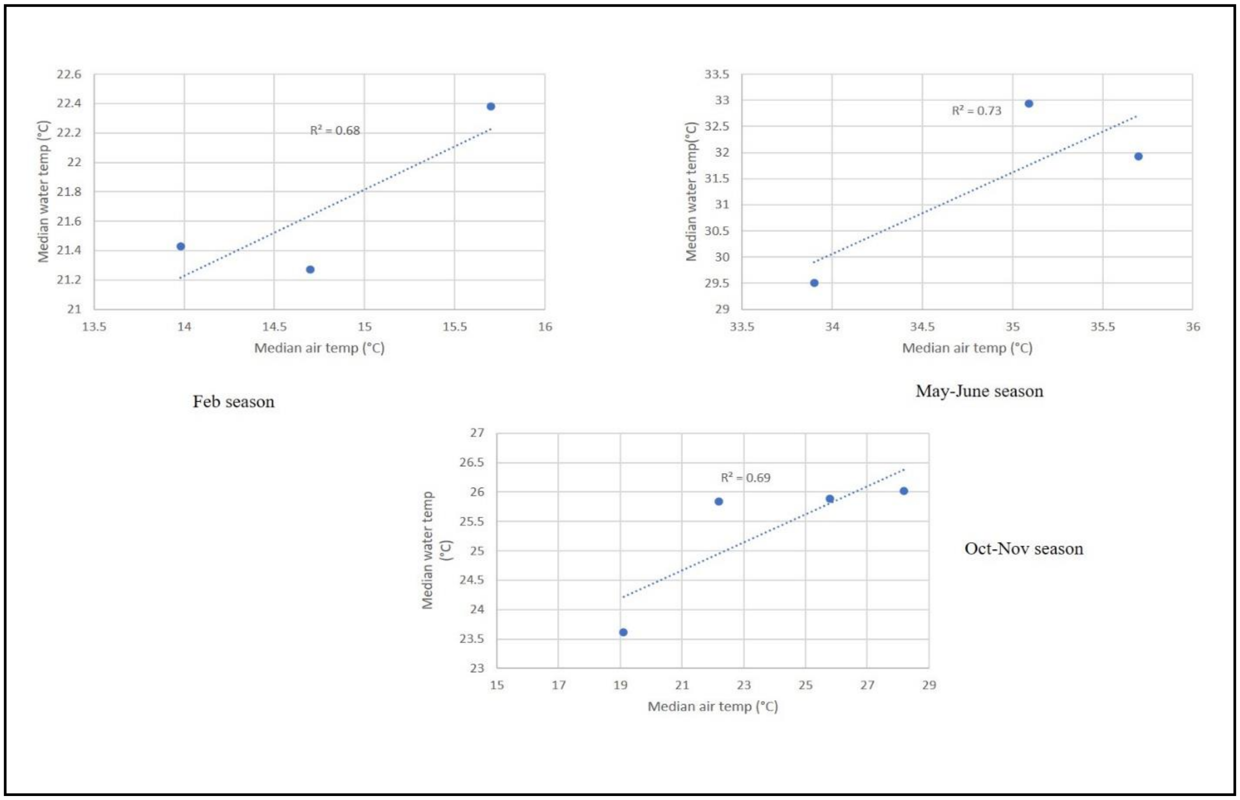

Figure 3.36 Season-wise meadin air temp and water surface temp for L-7 datasets

3.6 Discussion

The long-term temperature analysis of the river Ganga will give a clear overview of how temperature variation has occurred throughout the stretch (Mirzapur to Ghazipur) of approximately 230 kilometers for the years 2013, 2015, 2017, and 2018. Conventional methods of calculating the surface water temperature can be done only at sparse locations, as this is very much time-consuming. Two different satellites, namely LANDSAT-7 and LANDSAT-8 thermal data, have been used for generating a thermal profile. By observing the longitudinal profile generated from the LANDSAT7 satellite, it can be seen that several data gaps have existed because of scan line error, but continuous data has been obtained from L8 as there is no such error.

By looking at Figure 3.37, scan line error can be appropriately seen for the LANDSAT-7 thermal as well RGB (Red Green Blue) image. Figure 3.38 shows that there is no scan line problem for LANDSAT-8 thermal and RGB images.

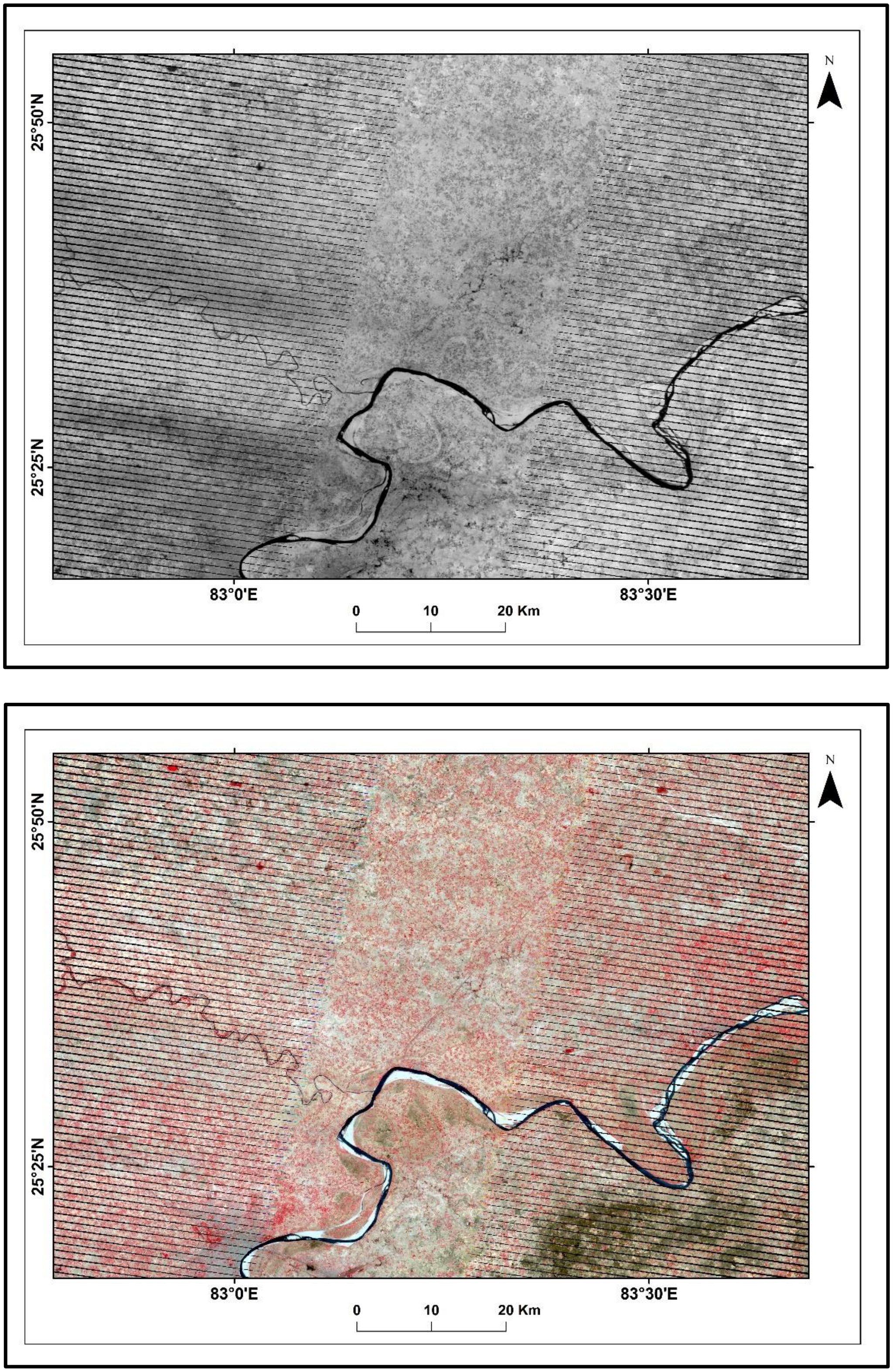

Figure 3.37 Thermal and RGB image of a LANDSAT-7 scene; Ghazipur situated in the non-scan line region

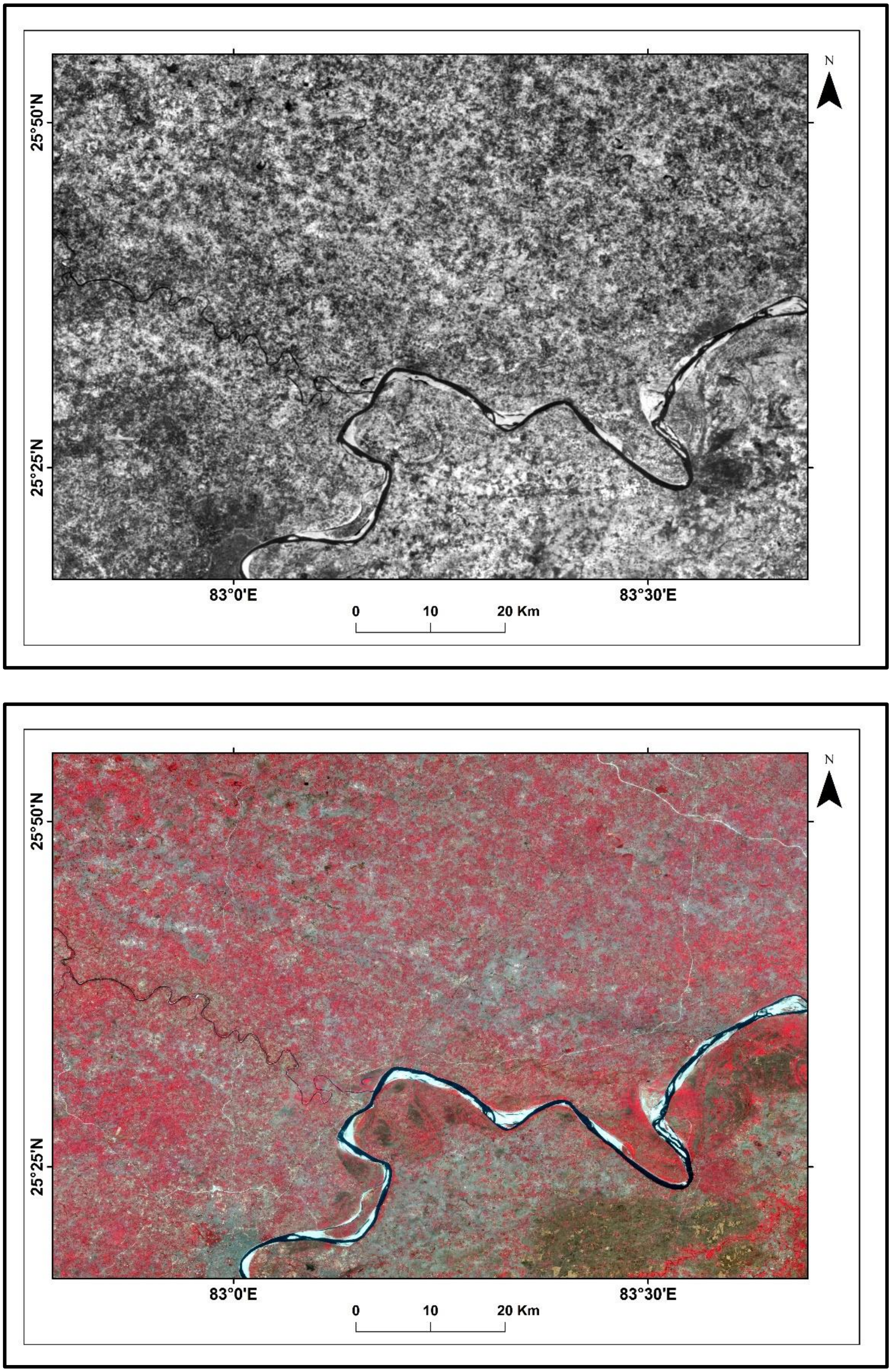

Figure 3.38 Thermal and RGB image of a LANDSAT-8 scene

From the foregoing discussion, it could be stated that the river temperature has been affected by meteorological parameters such as air temperature, wind speed, and precipitation. The low wind speed values (Table 3.1 & 3.2) suggest that it doesn’t have much influence on river temperature in this study. The simultaneous analysis of longitudinal temperature profile and precipitation data available for the three consecutive days up to data acquisition makes it apparent that the temperature profile for May and June registers a dip in the case of precipitation on two subsequent days of data acquisition. Such a pattern has been observed for the LANDSAT-7 imagery for May 2013 and LANDSAT-8 imageries for May 2018, June 2015, and June 2017.

It is quite evident from Table 3.3 that the air temperature has a better relationship with the LANDSAT-8 estimated temperature in comparison to LANDSAT-7, but the spatial resolution of thermal bands in LANDSAT-7 is better than that of LANDSAT-8. This phenomenon is attribute to the bandwidth of the thermal band in LANDSAT-7, which is much more, i.e., it ranges from 10.31-12.36µm (micrometer) in comparison to thermal band 10 of LANDSAT-8, i.e., it ranges from 10.60-11.19µm. So, the band having more bandwidth is more prone to be, affected by the stray values. Thus, the relationship between LANDSAT-8 satellite estimated temperature with air temperature is much better. Air temperature shows a weak correlation with water temperature. The IMD measures the air temperature values. From Table 3.3**,** it is quite obvious that the correlation is comparatively weak for the satellite estimated temperature and air temperature for the month of February because the daily minimum temperature of the air is very low, and surface water temperature is much higher. This is due to the fact that the convection current flowing inside the water makes the water warm. Similarly, for the month of October-November, the correlation value is poor. During the summer season, i.e., for May-

June, the daily minimum temperature is not as low as surface water temperature, so the correlation for the summer season is comparatively better for these two satellites. The thermal profile of river centerline has been calculated. It is worth mentioning that the median value with a 3x3 window size has been considered for computing the river temperature longitudinal profile because the median is statistically more dynamic and less affected by stray values as compared to mean values.

The minimum temperature in February is noticeably lower than in November for all the years under consideration.

The aquatic organism can endure a specific temperature range (Caissie, 2006; Subehi et al., 2010), therefore, the analysis of seasonal variation of river temperature profiles over a spatial extent can be quite valuable for studying the rate of chemical reaction, which in turn impact the aquatic ecology of the rivers. Therefore, an in-depth study covering long periods is much desired after undertaking the river thermal profile.